Atmos. Chem. Phys., 22, 13753–13782, 2022
https://doi.org/10.5194/acp-22-13753-2022

Atmospheric Chemistry and Physics
Open Access
EGU

Global tropospheric ozone trends, attributions, and radiative impacts in 1995–2017: an integrated analysis using aircraft (IAGOS) observations, ozonesonde, and multi-decadal chemical model simulations

Haolin Wang[1,2], Xiao Lu[1,2], Daniel J. Jacob[3], Owen R. Cooper[4,5], Kai-Lan Chang[4,5], Ke Li[6], Meng Gao[7], Yiming Liu[1,2], Bosi Sheng[1], Kai Wu[8], Tongwen Wu[9,10], Jie Zhang[9,10], Bastien Sauvage[11], Philippe Nédélec[11], Romain Blot[11], and Shaojia Fan[1,2]

[1]School of Atmospheric Sciences, Sun Yat-sen University, Zhuhai, Guangdong, China
[2]Guangdong Provincial Observation and Research Station for Climate Environment and Air Quality Change in the Pearl River Estuary, Key Laboratory of Tropical Atmosphere-Ocean System, Ministry of Education, Southern Marine Science and Engineering Guangdong Laboratory (Zhuhai), Zhuhai, Guangdong, China
[3]Harvard John A. Paulson School of Engineering and Applied Sciences, Harvard University, Cambridge, MA, USA
[4]Cooperative Institute for Research in Environmental Sciences, University of Colorado Boulder, Boulder, CO, USA
[5]NOAA Chemical Sciences Laboratory, Boulder, CO, USA
[6]Jiangsu Key Laboratory of Atmospheric Environment Monitoring and Pollution Control, Collaborative Innovation Center of Atmospheric Environment and Equipment Technology, School of Environmental Science and Engineering, Nanjing University of Information Science & Technology, Nanjing, China
[7]Department of Geography, Hong Kong Baptist University, Hong Kong SAR, China
[8]Department of Land, Air, and Water Resources, University of California Davis, Davis, CA, USA
[9]CMA Earth System Modeling and Prediction Centre, Beijing, China
[10]State Key Laboratory of Severe Weather, Beijing, China
[11]Laboratoire d'Aérologie (LAERO), Université Toulouse III – Paul Sabatier, CNRS, Toulouse, France

Correspondence: Xiao Lu (luxiao25@mail.sysu.edu.cn) and Shaojia Fan (eesfsj@mail.sysu.edu.cn)

Received: 30 May 2022 – Discussion started: 5 July 2022
Revised: 22 September 2022 – Accepted: 30 September 2022 – Published: 25 October 2022

Abstract. Quantification and attribution of long-term tropospheric ozone trends are critical for understanding the impact of human activity and climate change on atmospheric chemistry but are also challenged by the limited coverage of long-term ozone observations in the free troposphere where ozone has higher production efficiency and radiative potential compared to that at the surface. In this study, we examine observed tropospheric ozone trends, their attributions, and radiative impacts from 1995–2017 using aircraft observations from the In-service Aircraft for a Global Observing System database (IAGOS), ozonesondes, and a multi-decadal GEOS-Chem chemical model simulation. IAGOS observations above 11 regions in the Northern Hemisphere and 19 of 27 global ozonesonde sites have measured increases in tropospheric ozone (950–250 hPa) by 2.7 ± 1.7 and 1.9 ± 1.7 ppbv per decade on average, respectively, with particularly large increases in the lower troposphere (950–800 hPa) above East Asia, the Persian Gulf, India, northern South America, the Gulf of Guinea, and Malaysia/Indonesia by 2.8 to 10.6 ppbv per decade. The GEOS-Chem simulation driven by reanalysis meteorological fields and the most up-to-date year-specific anthropogenic emission inventory reproduces the overall pattern of observed tropospheric ozone trends, including the large ozone increases over the tropics of 2.1–2.9 ppbv per decade and above East Asia of 0.5–1.8 ppbv per decade and the weak tropospheric ozone trends above North

America, Europe, and high latitudes in both hemispheres, but trends are underestimated compared to observations. GEOS-Chem estimates an increasing trend of 0.4 Tg yr^{-1} of the tropospheric ozone burden in 1995–2017. We suggest that uncertainties in the anthropogenic emission inventory in the early years of the simulation (e.g., 1995–1999) over developing regions may contribute to GEOS-Chem's underestimation of tropospheric ozone trends. GEOS-Chem sensitivity simulations show that changes in global anthropogenic emission patterns, including the equatorward redistribution of surface emissions and the rapid increases in aircraft emissions, are the dominant factors contributing to tropospheric ozone trends by 0.5 Tg yr^{-1}. In particular, we highlight the disproportionately large, but previously underappreciated, contribution of aircraft emissions to tropospheric ozone trends by 0.3 Tg yr^{-1}, mainly due to aircraft emitting NO_x in the mid-troposphere and upper troposphere where ozone production efficiency is high. Decreases in lower-stratospheric ozone and the stratosphere–troposphere flux in 1995–2017 contribute to an ozone decrease at mid-latitudes and high latitudes. We estimate the change in tropospheric ozone radiative impacts from 1995–1999 to 2013–2017 is +18.5 mW m^{-2}, with 43.5 mW m^{-2} contributed by anthropogenic emission changes (20.5 mW m^{-2} alone by aircraft emissions), highlighting that the equatorward redistribution of emissions to areas with strong convection and the increase in aircraft emissions are effective for increasing tropospheric ozone's greenhouse effect.

1 Introduction

Tropospheric ozone is a major air pollutant that has a detrimental effect on human physiology and ecosystem productivity and controls the oxidizing capacity of the troposphere as the dominant source of hydroxyl radicals (OH) (Atkinson, 2000; Jacob, 2000; Monks et al., 2015; Fleming et al., 2018; Unger et al., 2020). It is also a short-lived climate forcer interacting with both solar (shortwave, SW) and terrestrial (longwave, LW) radiation (IPCC, 2021). Tropospheric ozone is produced chemically from anthropogenic and natural precursors; it is also transported from the stratosphere and is removed by chemical loss and dry deposition. The ozone lifetime spans from hours in the polluted boundary layer to a few weeks in the free troposphere, sufficiently short that ozone distributions and trends are highly variable. Chemistry climate models indicate an increase in the tropospheric ozone burden since the 1990s (Skeie et al., 2020), and regional changes in tropospheric ozone levels are likely to be caused by shifts in anthropogenic emissions of ozone precursors (Zhang et al., 2016) and climate (Lin et al., 2014; Lu et al., 2019b). Chemical models have been extensively used for quantifying the drivers of ozone trends at individual sites or regions and for estimating ozone radiative impacts, but their applications to the continental and global scales are largely constrained by the limited coverage of robust long-term ozone measurements for evaluating modeled ozone trends, especially in the free troposphere (Gaudel et al., 2020) where ozone has greater radiative impacts than at the surface (Lacis et al., 1990; Hansen et al., 1997). Here, we integrate long-term aircraft ozone observations, ozonesonde measurements, and multi-decadal chemical model simulations to quantify global tropospheric ozone trends, their attributions, and the resulting radiative impacts for 1995–2017.

The first phase of the Tropospheric Ozone Assessment Report (TOAR-I) initiated in 2014 utilized available surface, ozonesonde, aircraft, and satellite observations to assess tropospheric ozone trends from 1970 to 2014 (Schultz et al., 2017). TOAR-I concluded that observations through 2014 were not sufficient to detect an unambiguous trend in global tropospheric ozone burden over the past 2 decades (Gaudel et al., 2018). The Intergovernmental Panel on Climate Change Sixth Assessment Report (IPCC; AR6; Sect. 2.2.5.3) assessed the historical ozone records from the early and mid-20th century to the present day (Gulev et al., 2021), concluding that

> Based on sparse historical surface/low altitude data tropospheric ozone has increased since the mid-20th century by 30 %–70 % across the NH (medium confidence). Surface/low altitude ozone trends since the mid-1990s are variable at northern mid-latitudes, but positive in the tropics (2 % to 17 % per decade) (high confidence). Since the mid-1990s, free tropospheric ozone has increased by 2 %–7 % per decade in most regions of the northern mid-latitudes, and 2 %–12 % per decade in the sampled regions of the northern and southern tropics (high confidence). Limited coverage by surface observations precludes identification of zonal trends in the SH, while observations of tropospheric column ozone indicate increases of less than 5 % per decade at southern mid-latitudes (medium confidence).

An updated assessment from Cooper et al. (2020) reported a range of positive and negative ground-level ozone trends from 1995 to 2018 at 27 globally distributed remote sites. However, these sites represent less than 25 % of the global surface area and are not indicative of the free troposphere. Ozonesondes provide measurements in the free troposphere, but their representativeness of regional trends is largely limited by the low sampling frequency (2–3 times per week or

lower) and their sparse spatial coverage on the continental scale (Tarasick et al., 2019; Chang et al., 2022). Satellite instruments provide high-resolution observations of tropospheric column ozone with excellent spatial coverage. Long-term tropospheric ozone trends from limited satellite products indicate increases across the tropics since the 1980s and 1990s (Ziemke et al., 2019; Gulev et al., 2021), but satellite-detected trends at mid-latitudes since the early 2000s are less certain due to instrument errors (e.g., row anomaly), uncertainties in retrieval algorithms, and disagreements between the available products (Gaudel et al., 2018). Ozone measurements from the In-service Aircraft for a Global Observing System database (IAGOS) (Petzold et al., 2015), which contains ozone profiles from more than 60 000 commercial aircraft flights worldwide since 1994, are a critical source of data for quantifying ozone trends in the free troposphere (Cohen et al., 2018). A recent study utilizing IAGOS observations identified remarkable ozone increases in the free troposphere since 1994 above multiple regions of the Northern Hemisphere (Gaudel et al., 2020). The IAGOS observations provide a new opportunity for checking the consistency of ozone trends derived from other observation platforms (e.g., ozonesondes) and for evaluating the performance of chemical models used for interpreting ozone trend attributions and radiative impacts.

Modeling studies attributing long-term ozone trends have largely concentrated on the ground level and on individual sites or regions of the US and Europe where extensive surface observations are available (Parrish et al., 2014; Yang et al., 2014; Lin et al., 2017; Lu et al., 2018; Xu et al., 2018; Yan et al., 2018), while analyses of tropospheric ozone trend attribution on larger scales are rather limited. Zhang et al. (2016) showed that increases in the simulated global tropospheric ozone burden between 1980 and 2010 were dominated by the equatorward redistribution of anthropogenic emissions to developing regions in the tropics, particularly in East Asia and South Asia. The rise in tropospheric ozone burden over the past 2 decades was also reproduced in models from the Coupled Model Intercomparison Project Phase 6 (CMIP6) (Griffiths et al., 2021), but quantification of ozone trend drivers was not available. Lu et al. (2019b) revealed that the ozone increases in the Southern Hemisphere troposphere over 1990–2010 were linked to the poleward expansion of the Hadley circulation and associated changes in transport patterns and ozone production efficiency. The sparsity of available concurrent observations hindered a more comprehensive evaluation of simulated ozone trends in all of the above analyses and thus limits the interpretation of model results. We also lack an updated quantitative evaluation of anthropogenic and climatic drivers of global and continental ozone trends for years after 2010, when anthropogenic emissions of ozone precursors show contrasting changes compared to earlier years in regions such as China (Zheng et al., 2018). Estimates of ozone radiative impacts in previous studies are relative to the pre-industrial period (Stevenson et al., 2013; Skeie et al., 2020) and are poorly constrained by long-term ozone measurements in the troposphere, with no reliable ozone observations prior to the 20th century (Tarasick et al., 2019).

In this study, we aim to update our understanding of tropospheric ozone trends, their attributions, and attendant radiative impacts on the global scale for the period 1995–2017 from chemical model simulations evaluated against extensive long-term ozone measurements. We focus on the years 1995–2017 when ozone measurements in the free troposphere become increasingly available and state-of-the-science gridded anthropogenic emission inventories are reliable. We use the GEOS-Chem chemical transport model driven by assimilated meteorological fields and the most up-to-date global anthropogenic emission inventory to interpret tropospheric ozone trends for this period. We evaluate the GEOS-Chem tropospheric ozone trends with the aircraft ozone observations from the IAGOS database which provides long-term ozone measurements in multiple regions, together with ozonesonde measurements; we also compare the GEOS-Chem results with CMIP6 models. We then conduct a series of sensitivity simulations to quantify the impact of anthropogenic emissions and climate change on global and continental tropospheric ozone trends and estimate the resulting radiative impacts.

2 Materials and methods

2.1 IAGOS observations

The IAGOS program is a European Research Infrastructure (data available at https://www.iagos.org/, last access: 9 March 2022) initiated in August 1994 (Thouret et al., 1998) that measures atmospheric composition worldwide using instruments on board commercial aircraft of internationally operating airlines (Nédélec et al., 2015). Ozone is measured using a dual-beam ultraviolet absorption monitor with a time resolution of 4 s, a precision of ± 2 %, and an accuracy of about ± 2 nmol mol^{-1} (Thouret et al., 1998; Nédélec et al., 2015). IAGOS data have been regularly calibrated and show internal consistency for the duration of the program (Blot et al., 2021). Measurements are made at any time of the day, during takeoff and landing, and during the cruise portion of the flight. The sampling frequency varies depending on the airline schedule but can be as high as 4 profiles d^{-1} in regions such as western Europe, enabling a robust estimate of changes in free tropospheric ozone. Evaluations of IAGOS data show that they are consistent with ozonesonde records in the upper troposphere–lower stratosphere above western Europe (Staufer et al., 2013, 2014) and are representative of ozone in the lower troposphere (Petetin et al., 2018; Cooper et al., 2020). Previous studies have applied IAGOS data to estimate regional-scale tropospheric ozone trends from the northern mid-latitudes to the tropics (Cohen et al., 2018; Cooper et al., 2020; Gaudel et al., 2020).

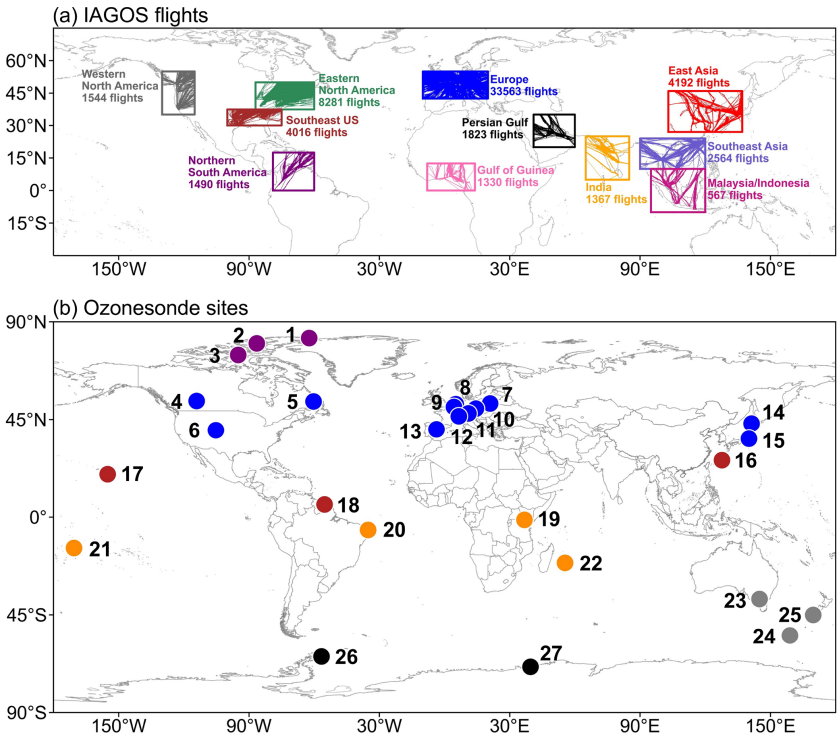

Figure 1. IAGOS and ozonesonde measurements of tropospheric ozone used in this study. The upper panel shows the map of the 11 study regions with frequent IAGOS sampling between 1995 and 2017 (grouped by color). The flight tracks are indicated in the boxes showing western North America, eastern North America, Europe, East Asia (including northern China, the Korean Peninsula, and part of Japan), the Southeast United States, northern South America, the Gulf of Guinea, the Persian Gulf, India, Southeast Asia, and Malaysia/Indonesia. The lower panel shows the location of selected ozonesonde sites in 1995–2017 used in this study, grouped by six latitude bands with an interval of 30° as denoted by different colors.

We focus on 11 regions with extensive IAGOS ozone profile sampling between 1995 and 2017, following Gaudel et al. (2020), as illustrated in Fig. 1a, to estimate tropospheric ozone trends; to the best of our knowledge this is the first time that IAGOS data have been used to evaluate long-term (> 20 years) tropospheric ozone trends in a global chemistry transport model. These 11 study regions have frequent sampling in both the early (1995–2004) and late periods (2011–2017) between 1995 and 2017, allowing the estimation of tropospheric ozone trends over periods spanning 2 decades (see Sect. 2.5). As shown in Fig. 1, western Europe is the region with the most frequent IAGOS ozone sampling with 33 563 available ozone profiles between 1995 and 2017, followed by eastern North America (8281 profiles), East Asia (4192 profiles), the Southeast US (4016 profiles), and Southeast Asia (2564 profiles). All regions except for Malaysia/Indonesia (567 flights) have more than 1000 ozone profiles in this period. The inclusion of IAGOS data in Asia, Africa, and South America provides a unique opportunity to evaluate and interpret tropospheric ozone trends in these developing regions.

2.2 Ozonesonde observations

We also use ozonesonde measurements from the World Ozone and Ultraviolet Radiation Data Centre (WOUDC; available at https://woudc.org/data.php, last access: 16 October 2022). WOUDC is operated by the Meteorological Service of Canada, within Environment and Climate Change Canada. For our study period of 1995–2017, the database contains ozone profiles from 130 globally distributed sites. Ozone from the surface to the stratosphere (from launch up to 35 km) is measured by balloon-borne ozone electrochemical concentration cell instruments (Tarasick et al., 2019) with a vertical resolution of about 100 m and an accuracy of 5 %–15 % in the troposphere and 5 % in the stratosphere (Sterling et al., 2018; Witte et al., 2018; Steinbrecht et al., 2021). The sampling frequencies of ozonesondes vary across sites but are mostly lower than 2–4 profiles per week, posing a challenge for our ability to detect a trend. Chang et al. (2020) estimated that 18 profiles per month are required for accurate and robust long-term trend quantification at a single monitoring station. As very few monitoring locations can achieve such sampling frequencies, we soften the criteria to have (1) at least 3 observations per month for calculating the monthly mean, (2) at least 2 monthly observations for the seasonal

mean and at least 8 months for annual mean, and (3) at least 15 annual mean observations for the period of 1995–2017. Ozonesonde sites that meet these criteria and used in this study are presented in Fig. 1b and Table 1, including 18 and 9 ozonesonde sites in the Northern Hemisphere and Southern Hemisphere, respectively. These stations have been used to study tropospheric ozone trends in North America, Europe, Japan, and the Southern Hemisphere (Oltmans et al., 2013; Tarasick et al., 2016; Zeng et al., 2017; Lu et al., 2019b; Kumar et al., 2021; Chang et al., 2022).

2.3 GEOS-Chem model description and configuration

We apply the global three-dimensional chemical transport model GEOS-Chem version 13.3.1 (available at https://github.com/geoschem/GCClassic/tree/13.3.1, last access: 9 March 2022, Bey et al., 2001) to interpret global tropospheric ozone and its trends for 1995–2017. The model is driven by Modern-Era Retrospective analysis for Research and Application version 2 (MERRA-2) assimilated meteorological fields from the NASA Global Modeling and Assimilation Office (GMAO), which has a native horizontal resolution of 0.5°(latitude) × 0.625°(longitude) and 72 vertical layers extending from the surface to 0.01 hPa (Gelaro et al., 2017).

GEOS-Chem describes coupled ozone–NO_x–VOCs–aerosol–halogen tropospheric (volatile organic compounds; Wang et al., 1998; Park et al., 2004; Parrella et al., 2012; Mao et al., 2013) and stratospheric chemistry (Eastham et al., 2014). The model prescribes methane at the surface on the basis of spatially interpolated monthly mean surface methane observations from the NOAA Global Monitoring Division in 1995–2017 and allows for its transport and chemistry (Murray, 2016). Gridded monthly surface mixing ratios for N_2O, CFCs (chlorofluorocarbons), HCFCs (hydrochlorofluorocarbons), halons, and organic chlorine species for 1995–2017 are obtained from the World Meteorological Organization (Daniel et al., 2007) and are used as boundary conditions for these species in the model. The chemical kinetics are from the Jet Propulsion Laboratory (JPL) and International Union of Pure and Applied Chemistry (IUPAC) (Sander et al., 2011; IUPAC, 2013). Photolysis rates are calculated by the Fast-JX scheme (Bian and Prather, 2002). Advection of tracers in GEOS-Chem is performed using the TPCORE advection algorithm (Lin and Rood, 1996). The boundary layer mixing process is described by a non-local scheme (Lin and McElroy, 2010). Dry deposition of both gas and aerosols is calculated by a resistance-in-series algorithm (Wesely, 1989; Zhang et al., 2001), with updates in ozone deposition to the ocean as described by Pound et al. (2020). Wet deposition for water-soluble aerosols and gases is described by Liu et al. (2001) and Amos et al. (2012).

Emissions in GEOS-Chem are operated by the Harvard–NASA Emission Component (HEMCO) (Keller et al., 2014). We apply the latest version of the Community Emissions Data System inventory (CEDSv2), which builds on the extension of the CEDS system to 2017 as described in McDuffie et al. (2020), to provide year-specific global anthropogenic emissions for 1995–2017 in GEOS-Chem (O'Rourke et al., 2021). The early version of this emission inventory, $CEDS_{CMIP6}$, provided gridded (0.5° × 0.5°) monthly emissions of reactive gases and aerosols from 1750 to 2014 (Hoesly et al., 2018) and was used in the CMIP6 experiment (Eyring et al., 2016; Hoesly et al., 2018). The $CEDS_{CMIP6}$ emissions from European countries, the US, Canada, and Australia are scaled to emissions from well-developed regional emission inventories, including the European Monitoring and Evaluation Programme (EMEP) (EMEP, 2016), the US National Emissions Inventory (NEI) (US EPA, 2016), Canadian Air Pollutant Emissions Inventory (APEI) (ECCC, 2016), and Australian National Pollutant Inventory (NPI) (ADE, 2016). As for Asia, the $CEDS_{CMIP6}$ is scaled to an updated version of the MIX inventory for China (Li et al., 2017) and the Regional Emissions Inventory in Asia (REAS) for other areas in Asia (Kurokawa et al., 2013). Here CEDSv2 updates activity data for combustion- and process-level emission sources and incorporates new regional inventories for India (Venkataraman et al., 2018) and Africa (Marais and Wiedinmyer, 2016). In addition, CEDSv2 emissions are also scaled to the latest EMEP (EMEP, 2019), NEI (US EPA, 2019), APEI (ECCC, 2019), NPI (ADE, 2019), and MEIC (Multi-resolution Emission Inventory for China; Zheng et al., 2018) emission inventories for Europe, the US, Canada, Australia, and China, respectively, enabling the extension of emission estimates to 2017.

Figure 2 presents the evolution of global anthropogenic NO_x, CO, and NMVOC (non-methane volatile organic compound) emissions and the spatial distributions of their trends in 1995–2017 from the CEDSv2 used in this study. Global anthropogenic NO_x emissions showed increases from 34.5 TgN in 1995 to 40.5 TgN in 2008, then leveled off from 2008 to 2012, and decreased afterward to 36.2 TgN in 2017. Global anthropogenic CO emissions decreased from 1995 at 648.6 Tg, leveled off between 2002 and 2012, and decreased again afterward to 539 Tg in 2017. Global anthropogenic NMVOC emissions showed increases from 133.8 Tg in 1995 to 149.3 Tg in 2012 and then flattened afterwards. Linear trends in global anthropogenic NO_x, CO, and NMVOC emissions are 0.58 TgN yr^{-1}, −2.7 Tg yr^{-1}, and 0.96 Tg yr^{-1}, respectively. Inspection of the regional trends shows that the global anthropogenic emissions have shifted from developed regions in the northern mid-latitudes such as Europe and North America, where regulations of anthropogenic emissions were implemented in the 1990s (Archibald et al., 2017), to developing regions in the tropics and subtropics. The regions with the largest increases in anthropogenic emissions are East Asia and South Asia, the Middle East, and Africa. The decline in global anthropogenic NO_x and CO emissions after 2012 is largely driven by emission reduction in China associated with the implementation of emission con-

Table 1. List of the monitoring ozonesonde stations.

No.	Site	Region	Latitude (°)	Longitude (°)	Elevation (m)	Sample frequency (per month)
1	Alert	Canada	82.5	−62.3	210	4.0
2	Eureka	Canada	80.05	−86.42	610	5.6
3	Resolute	Canada	74.72	−94.98	64	3.0
4	Edmonton	Canada	53.55	−114.10	766	4.0
5	Goose Bay	Canada	53.30	−60.39	39	3.9
6	Boulder ESRL HQ (CO)	United States	39.99	−105.26	1634	4.5
7	Legionowo	Poland	52.40	20.97	96	4.5
8	De Bilt	Netherlands	52.10	5.18	2	4.4
9	Uccle	Belgium	50.80	4.36	100	12.2
10	Prague	Czech Republic	50.01	14.45	302	4.0
11	Hohenpeissenberg	Germany	47.80	11.01	985	10.6
12	Payerne	Switzerland	46.81	6.94	490	12.8
13	Madrid	Spain	40.45	−3.72	680	3.7
14	Sapporo	Japan	43.06	141.33	26	3.7
15	Tateno (Tsukuba)	Japan	36.10	140.13	31	4.3
16	Naha	Japan	26.20	127.68	27	3.5
17	Hilo (HI)	Northeastern Pacific	19.58	−155.07	11	5.8
18	Paramaribo	Suriname	5.81	−55.21	23	6.2
19	Nairobi	Kenya	−1.30	36.75	1795	3.8
20	Natal	Brazil	−6.00	−35.20	0	3.1
21	Samoa (Cape Matatula)	Southeastern Pacific	−14.25	−170.56	77	4.4
22	La Réunion	Southwestern Indian Ocean	−21.08	55.38	2160	3.1
23	Broadmeadows	Australia	−37.69	144.95	108	3.8
24	Macquarie Island	Australia	−54.50	158.94	6	3.7
25	Lauder	New Zealand	−45.04	169.68	370	4.3
26	Marambio	Antarctica	−64.24	−56.62	198	4.6
27	Syowa	Antarctica	−69.00	39.58	21	4.6

ESRL HQ: Earth System Research Laboratories headquarters.

trol strategies, while NMVOC emissions are not effectively mitigated (Zheng et al., 2018).

Figures 2 and S1 also compare the anthropogenic emission trends from CEDSv2 and $CEDS_{CMIP6}$ for 1995–2014. We find that the anthropogenic NO_x and CO emissions from CEDSv2 are lower than those in the $CEDS_{CMIP6}$ inventory in particular for years after 2007 by 8.8 % and 3.9 %, respectively. This leads to a much smaller trend of global anthropogenic NO_x and CO in CEDSv2 ($0.58\,TgN\,yr^{-1}$ and $-2.7\,Tg\,yr^{-1}$) compared to those in $CEDS_{CMIP6}$ ($1.1\,TgN\,yr^{-1}$ and $0.32\,Tg\,yr^{-1}$) for 1995–2014. Anthropogenic NMVOC emissions are also smaller in CEDSv2 than $CEDS_{CMIP6}$ (150.1 Tg vs. 164.6 Tg in the year 2014). These differences mainly reflect the updated regional inventory for China (Zheng et al., 2018), along with the inclusion of regional inventories for DICE-Africa (Diffuse and Inefficient Combustion Emissions in Africa; Marais and Wiedinmyer, 2016) and SMoG-India (Speciated Multi-pollutant Generator; Venkataraman et al., 2018), as well as the updated activity data in CEDSv2 (Fig. S1 in the Supplement).

The default GEOS-Chem model includes a monthly three-dimensional gridded inventory of aircraft emissions of NO_x, CO, and hydrocarbons based on the Aviation Emissions Inventory Code v2.0 (AEIC) for the year 2005, resulting in 0.96 TgN of global aircraft NO emissions with no interannual variability. A new study has showed that aircraft activity has exploded in recent decades, with aircraft CO_2 emissions 79.8 % greater in 2018 relative to 1995 (Lee et al., 2021). Here we use the CEDS global aircraft emissions in 1995–2017 (O'Rourke et al., 2021), allowing for our simulation to capture the impact from increases in aircraft emissions on global ozone trends. The global aircraft emissions of NO_x, CO, and NMVOC estimates for 2005 in the CEDS inventory are 0.88 TgN, 0.54 Tg, and 0.08 Tg, respectively, slightly lower than those in the AEIC inventory. We find that the aircraft emissions of NO_x, CO, and NMVOCs increased from 1995 to 2017 by 0.51 TgN (76.2 %), 0.26 Tg (58.1 %), and 0.05 Tg (88.4 %), respectively (Fig. 2), consistent with Lee et al. (2021). Aircraft NO_x emissions account for only 3.3% of the total anthropogenic emissions in 2017; however, as we will see later, they play an important role in the global tropospheric ozone trends.

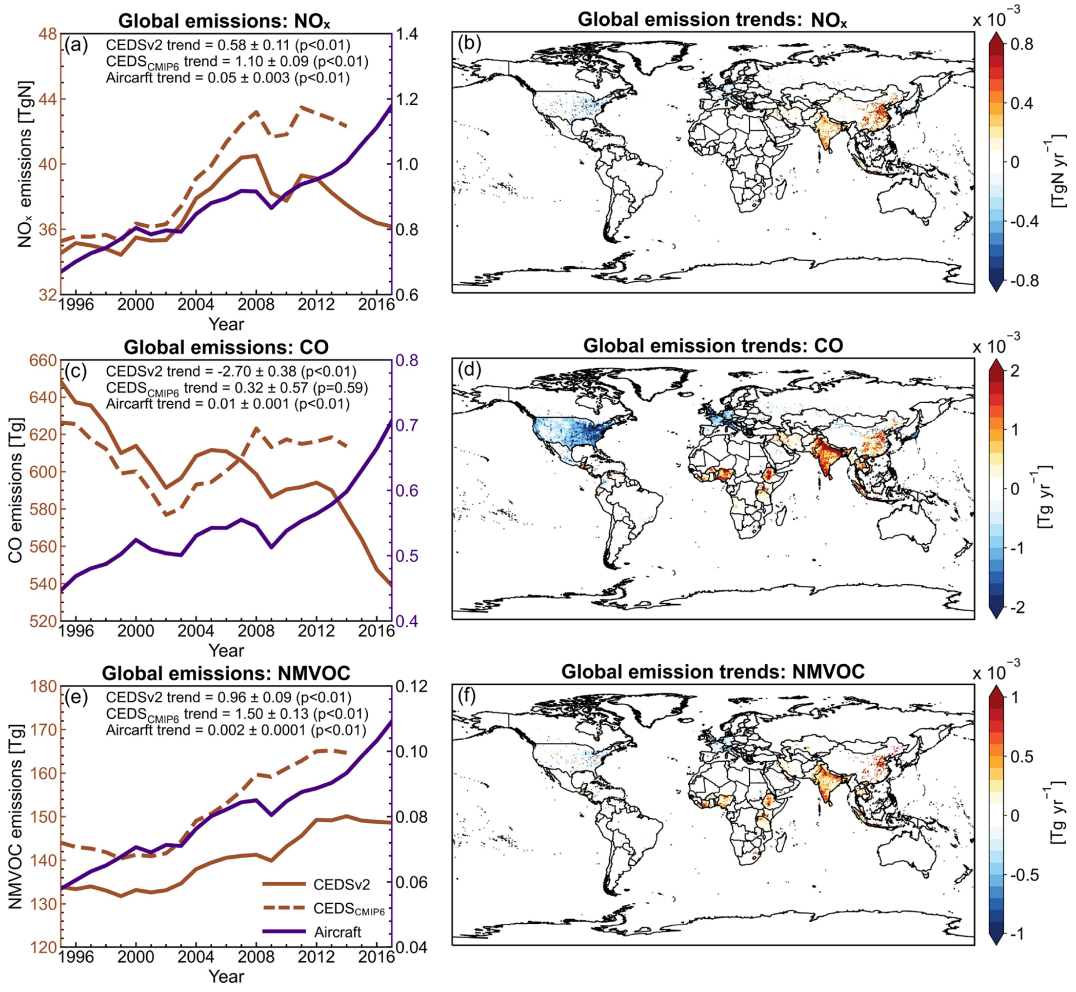

Figure 2. Trends in global annual anthropogenic (excluding aircraft emissions) and aircraft emissions of NO_x, CO, and NMVOCs from 1995 to 2017. **(a, c, e)** The total global anthropogenic NO_x, CO, and NMVOC emissions from the CEDSv2 and $CEDS_{CMIP6}$ inventories. **(b, d, f)** The spatial distribution of emission trends in the CEDSv2 inventory. Aircraft emissions are from O'Rourke et al. (2021). The total global anthropogenic emission trends with p values are shown in the left panels.

GEOS-Chem includes on-line calculation of biogenic emissions of NMVOCs and NO_x emissions from soil and lightning. Biogenic emissions are calculated using the Model of Emissions of Gases and Aerosols from Nature (MEGAN, version 2.1) (Guenther et al., 2012). Soil NO_x emissions are calculated based on the availability of nitrogen (N) in the soil and edaphic conditions such as soil temperature and moisture (Hudman et al., 2010, 2012; Lu et al., 2021). Lightning NO_x emissions are parameterized as a function of cloud-top height (Price and Rind, 1992) and are then vertically distributed according to Ott et al. (2010). The spatial pattern of lighting NO_x emissions is further constrained by climatological observations of lightning flash rates from the Lightning Imaging Sensor (LIS) and Optical Transient Detector (OTD) satellite instruments (Sauvage et al., 2007; Murray et al., 2012). Biomass burning emissions in 1995–2017 are from the BB4CMIP (historic global biomass burning emissions for CMIP6) inventory as described in van Marle et al. (2017), in which the emissions for years after 1997 are the same as the Global Fire Emissions Database version 4 (GFED4; van der Werf et al., 2017). Fire plumes can be injected beyond the planetary boundary layer (PBL). We partition 65 % of the biomass burning emissions to the PBL and the remaining 35 % into the free troposphere following Fischer et al. (2014) and Travis et al. (2016).

Model configurations are summarized in Table 2. We spin up the GEOS-Chem model by 10 years to provide an initial field for the atmospheric chemical components on 1 January 1995. The long spin-up time is to properly initialize the lower stratosphere. We conduct the standard simulation (BASE) from 1995 to 2017 using year-specific assimilated meteorology fields and anthropogenic and natural emissions as described above. We then conduct three sensitivity simulations to quantify the drivers of ozone trends. In the first

Table 2. Configurations of GEOS-Chem simulations in this study*.

Simulation	Aircraft emissions	Anthropogenic emissions	Biomass burning emissions	Global methane concentrations	Meteorology
BASE	V	V	V	V	V
FixAircraft	1995	V	V	V	V
FixAC	1995	1995	V	1995	V
FixABC	1995	1995	1995	1995	V

* "V" denotes those specific inputs vary interannually in the simulation, and "1995" denotes that the inputs are fixed to 1995 conditions. "FixAircraft" denotes only global aircraft emissions are fixed at 1995 levels in the simulation. "FixAC" denotes global anthropogenic emissions (including aircraft emissions) and the methane concentration level are fixed to 1995 conditions. "FixABC" denotes biomass burning emissions are fixed at 1995 levels based on FixAC.

sensitivity simulation, FixAC, we fix global anthropogenic emissions (including aircraft emissions) and methane concentration at 1995 levels. However, mixing ratios of ozone depletion species (CFCs, HCFCs) are not fixed, as such their influences on the stratospheric ozone are available in the FixAC simulation. Ozone trends in the FixAC thus estimate the influence of climate (including their impacts on natural emissions) and stratospheric ozone on tropospheric ozone trends. The difference in ozone trends between the BASE and FixAC simulation then quantifies the contributions of anthropogenic emissions of tropospheric ozone precursors (including aircraft emissions and methane) to ozone trends. In the second simulation, FixABC, we further fix biomass burning emissions at 1995 levels on the basis of FixAC, allowing us to examine the impact of biomass burning emissions alone on ozone trends. In the third simulation, FixAircraft, we fix global aircraft emissions at 1995 levels and use the difference in ozone trend between BASE and FixAircraft to estimate the contribution of aircraft emissions alone to ozone trends.

We run the GEOS-Chem model at a horizontal resolution of 4°(latitude) × 5°(longitude), with 72 vertical layers extending from the surface to 0.01 hPa. A 1-month model simulation at this resolution costs 4 h with 48 CPUs (http://wiki.seas.harvard.edu/geos-chem/index.php/GEOS-Chem_13.3.0#1-month_benchmarks, last access: 16 October 2021). Yielding 33-year (including 10-year spin-up simulation) global simulation of ozone trends thus requires computation time of more than 60 natural days. As such we do not use the finer resolution of 2° × 2.5° that would otherwise cost at least 8 times as much computational time and resources as in this study. This relatively coarse resolution of 4° × 5° may limit the ability of the model to capture finer-scale ozone trends, in particular near the surface where ozone and its precursor has a short lifetime. Artificial mixing of surface ozone precursors in coarse model grids may lead to higher-than-actual ozone production efficiency and therefore positive ozone biases which may further influence trend analyses (Wild and Prather, 2006; Yu et al., 2016; Young et al., 2018; Yin et al., 2021). The limitation of model resolution, however, should be alleviated for ozone in the free troposphere, where ozone has longer chemical lifetime and should be better mixed than near the surface (Petetin et al., 2016). In light of this we do not use surface ozone observations for model evaluation and mainly focus on the trend analyses above 950 hPa.

We also use model output from seven global climate–chemistry models in the CMIP6 historical experiments for comparison with the GEOS-Chem results and to examine the evolution of tropospheric ozone. An overview of the models included in this study is presented in Table 3. Model outputs are available on the Earth System Grid Federation (ESGF) website (https://esgf-node.llnl.gov/projects/cmip6/, last access: 9 March 2022). All the CMIP6 historical simulations of ozone for 1850–2014 apply the $CEDS_{CMIP6}$ inventory as the global anthropogenic emissions of air pollutants (Feng et al., 2020) and the BB4CMIP6 inventory as biomass burning emissions, and they apply the same external forcing from solar irradiance and well-mixed greenhouse gases (Meinshausen et al., 2017) but have significant differences in their resolutions, meteorology, chemical mechanisms, and representation of natural emissions such as lightning and biogenic emissions. The evolution of tropospheric ozone from 1850 to 2100 has been extensively analyzed in Griffiths et al. (2021). Here monthly model output of ozone for 1995–2014 is analyzed and compared with the GEOS-Chem results.

2.4 Trend estimation

We follow Gaudel et al. (2020) to determine tropospheric ozone trends from IAGOS and ozonesonde observations using the quantile regression method (Koenker and Bassett, 1978). The quantile regression method estimates trends based on the rank value of the sample distributions rather than the mean values, which makes no assumptions about the distribution of the data and has better tolerance to outliers (Koenker and Xiao, 2002; Chang et al., 2021). These advantages make it a robust tool for estimating trends of time series with many intermittent missing values, such as ozone records from the IAGOS and ozonesonde observations. More details of the method are described in Koenker and Hallock (2001).

Table 3. Information on the CMIP6 models used in this study.

No.	CMIP6 model[a]	Ensemble member[b]	Longitude × latitude	Vertical levels (top level)	Reference
1	BCC-ESM1	r1i1p1f1	∼ 2.8° × 2.8°	L26 (2.19 hPa)	Wu et al. (2020)
2	CESM2-WACCM	r1i1p1f1	∼ 1.25° × 0.9°	L70 (4.5×10^{-6} hPa)	Danabasoglu (2019b)
3	CESM2	r1i1p1f1	∼ 1.25° × 0.9°	L32 (2.25 hPa)	Danabasoglu (2019a)
4	GFDL-ESM4	r1i1p1f1	1.25° × 1°	L49 (0.01 hPa)	Krasting et al. (2018)
5	IPSL-CM6A-LR	r1i1p1f1	∼ 2.5° × 1.26°	L79 (0.01 hPa)	Boucher et al. (2018)
6	MPI-ESM-1-2-HAM	r1i1p1f1	∼ 1.8° × 1.8°	L47 (0.01 hPa)	Neubauer et al. (2019)
7	NorESM2-MM	r1i1p1f1	∼ 1.25° × 0.9°	L32 (0.03 hPa)	Bentsen et al. (2019)

[a] BCC-ESM1: Beijing Climate Center Earth System Model version 1. CESM2: Community Earth System Model version 2. WACCM: Whole Atmosphere Community Climate Model. GFDL-ESM4: Geophysical Fluid Dynamics Laboratory Earth System Model version 4. IPSL-CM6A-LR: Institut Pierre-Simon Laplace Climate Model 6A, low resolution. MPI-ESM-1-2-HAM: Max Planck Institute for Meteorology Earth System Model 1.2 coupled with the Hamburg Aerosol Module. NorESM2-MM: Norwegian Earth System Model 2, 1° resolution. [b] There are four indices defining an ensemble member: "r" for realization, "i" for initialization, "p" for physics, and "f" for forcing.

We calculate ozone trends on 15 pressure levels at 50 hPa intervals from 950 to 200 hPa for each IAGOS region and each ozonesonde site. We remove data points with ozone higher than 125 ppbv at altitudes higher than 500 hPa to exclude the influence from episodic stratospheric intrusions and because the effect of these intrusions is diluted in the model (Zhang et al., 2014), based on observed ozone values in fresh stratospheric intrusions and in air pollution plumes (Nowak et al., 2004; Cooper et al., 2005; Archibald et al., 2020). Following Gaudel et al. (2020), we first calculate the monthly mean ozone values to construct the mean seasonal cycle from 1995 to 2017 for each layer and for each IAGOS region or ozonesonde site. The mean seasonal cycle is then used to deseasonalize each ozone record at the same pressure level. Finally, the quantile regression method is applied to calculate the linear trend of ozone using all available deseasonalized ozone profiles at each pressure layer. We report linear trends of ozone at the 50th (median) and 95th quantile (in ppbv per decade) for the period 1995–2017 with a corresponding p value. Following the advice of the statistics community (Wasserstein et al., 2019) and as discussed in Gaudel et al. (2020), we do not use thresholds such as $p < 0.05$ to judge whether the reported trend is statistically significant.

2.5 Radiative-impact calculations

We use the radiative-kernel approach developed by Rap et al. (2015) to calculate the change in the radiative forcing of tropospheric ozone over the 1995–2017 period. The radiative kernel is defined as the derivative of the radiative flux relative to a small perturbation in ozone. We use the radiative kernel from Skeie et al. (2020), which is constructed using the University of Reading (UoR) radiative transfer model (Myhre et al., 2011). UoR calculates ozone radiative forcing using the Edwards and Slingo (1996) two-stream radiation scheme that includes eight bands in longwave (Myhre and Stordal, 1997) and six bands in shortwave bands (Stamnes et al., 1988). Ozone radiative kernels have been widely used in previous studies to compare the radiative forcing of ozone across different chemistry climate models (Rap et al., 2015; Iglesias-Suarez et al., 2018; Scott et al., 2018; Skeie et al., 2020). Iglesias-Suarez et al. (2018) showed that ozone radiative-forcing values calculated from the radiative-kernel technique and from the radiative transfer model are in good agreement with a global mean difference of 0.01 W m^{-2}. We interpolate the monthly ozone outputs from the GEOS-Chem simulations onto the T21 grid space (approximately 5.6° × 5.6°) and 60 vertical layers (ranging from the surface to 0.1 hPa) to match the resolution of the radiative kernel and then derive the radiative impacts.

3 Results and discussion

3.1 Evaluation of GEOS-Chem tropospheric ozone

We evaluate the simulated tropospheric ozone and trends from the GEOS-Chem BASE simulation with the IAGOS and ozonesonde measurements. We sample the model outputs along the flight and sonde tracks and apply the same processes to simulated values as observations.

Figure 3 compares the annual vertical ozone profiles with the IAGOS observations over the 11 regions in the Northern Hemisphere for the years 1995–1999 and 2013–2017. The model reproduces well the major features of tropospheric ozone vertical distributions, including the differences in the ozone increase with altitude between the northern midlatitudes and tropics. The model shows good agreement with IAGOS observations in terms of the absolute ozone levels over Europe and North America. Over East Asia, our GEOS-Chem simulation shows no significant ozone bias when averaging all IAGOS sampling data, but this reflects the offset between low bias in boreal spring and high bias in summer. Park et al. (2021) also reported the ozone underestimation from eight chemical models including GEOS-Chem above South Korea during the Korea–United States Air Quality (KORUS-AQ) campaign in May–June 2016, and Gaubert et al. (2020) attributed this to missing CO sources in emission inventories for East Asia. The modeled ozone is biased

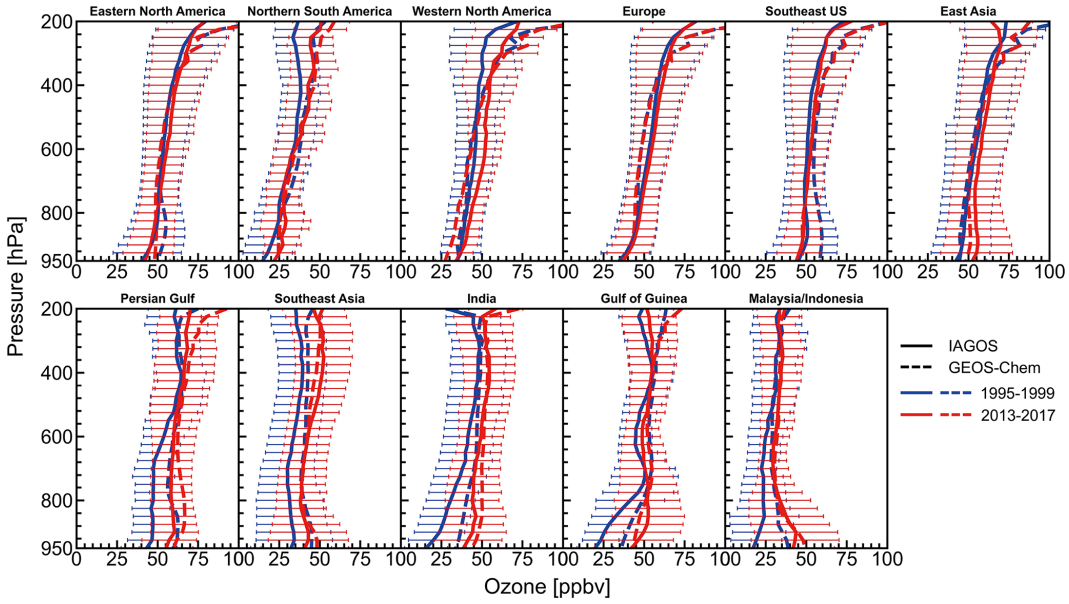

Figure 3. Comparison of IAGOS observations (solid line) and simulated (dashed line) ozone vertical profiles for 11 IAGOS regions from 1995–1999 (blue line) to 2013–2017 (red line). Horizontal bars are standard deviations in the observations.

high in the tropical regions particularly in boreal autumn and winter (Table S1 in the Supplement). We find that the GEOS-Chem ozone biases are smaller in 2013–2017 when activity data and emission factors are better constrained than in the early period of 1995–1999, smaller in regions where the CEDSv2 emission inventory is scaled to well-developed regional inventories (North America, Europe, East Asia) than in other regions, and larger in the lower troposphere than in the upper troposphere. In particular, the ozone low biases at the 950–800 hPa layer above tropical Asia and Africa are much larger (11.3–15.9 ppbv) in 1995–1999 than in 2013–2017 (about 2.5 ppbv). A possible reason is that anthropogenic emissions in the early period and in developing tropical regions are biased high, which will also lead to underestimation of tropospheric ozone trends over these regions, as will be discussed later.

Figure 4 further compares the simulated vertical distributions of ozone with the ozonesonde measurements. We aggregate the ozonesonde data into six latitudinal bands for comparison, and results for individual sites are shown in Fig. S2. The comparison again shows that GEOS-Chem captures the vertical structure of ozone at these globally distributed ozonesonde stations, but unlike the positive bias relative to IAGOS observations over industrialized areas, GEOS-Chem shows negative ozone biases in the free troposphere relative to ozonesonde measurement, in particular for remote sites in the extratropical regions by up to 20 ppbv. IAGOS and ozonesonde observations have very different spatial distributions (except overlaps in Europe) (Fig. 1) and reflect ozone difference over industrialized vs. remote regions so that inconsistency in simulated ozone bias can be expected. The low tropospheric ozone bias relative to ozonesonde observations in recent GEOS-Chem model versions has been demonstrated in several studies. The latest comprehensive evaluation of global tropospheric ozone simulation using the version 10.1 of the model (Hu et al., 2017) found small low ozone biases compared to ozonesonde observations in the northern extratropical and polar regions, which were attributed to the underestimation of stratosphere–troposphere ozone exchange (STE) flux in that version of the model. The scientific updates since the version 10.1 (https://geos-chem.seas.harvard.edu/geos-new-developments, last access: 16 October 2022), including the implementation of halogen (Cl-Br-I) chemistry in versions 11-02 and 12.9 (Sherwen et al., 2016; Wang et al., 2021), update of heterogeneous NO_y chemistry in aerosols and clouds in version 12.6 (Holmes et al., 2019), and introduction of oceanic ozone deposition in version 12.8 (Pound et al., 2020), have significantly improved the model performance for many other chemical species but tend to enlarge the ozone low bias; in particular updated halogen chemistry further decreases surface ozone in high-latitude regions (Wang et al., 2021). Correcting the ozone low bias in remote regions in GEOS-Chem would be a topic of future research.

3.2 Tropospheric ozone trends from observations and chemical models

We estimate tropospheric ozone trends over 1995–2017 using IAGOS and ozonesonde observations (Figs. 5–7 and S3). Figures 5 and S3 show the vertical distributions of annual tropospheric ozone trends at the 50th and 95th percentiles from IAGOS observations, estimated using the quantile regression

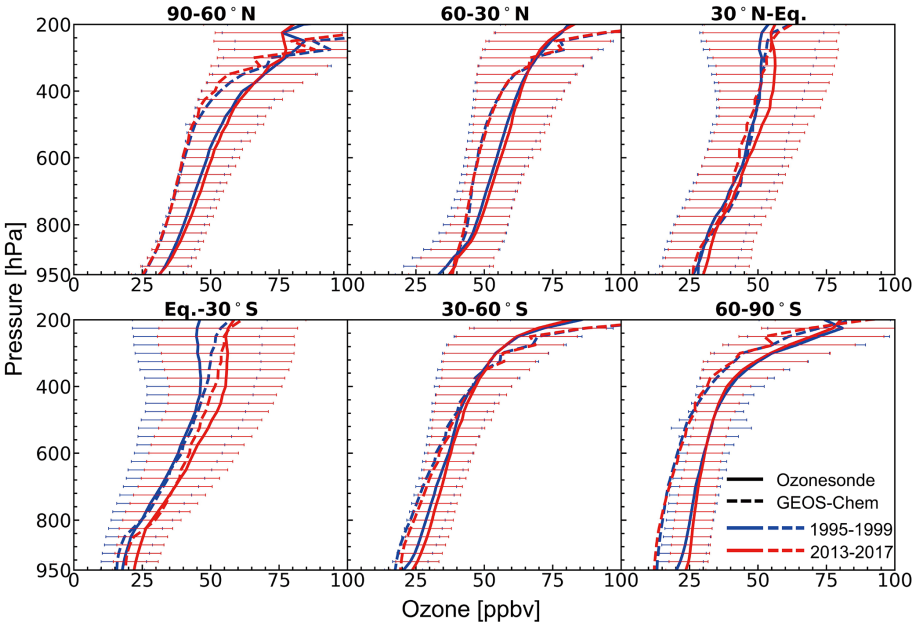

Figure 4. Comparison of ozonesonde (solid line) and simulated (dashed line) ozone vertical profiles for six zonal bands over 1995–1999 (blue line) and 2013–2017 (red line). Horizontal bars are standard deviations in the observation.

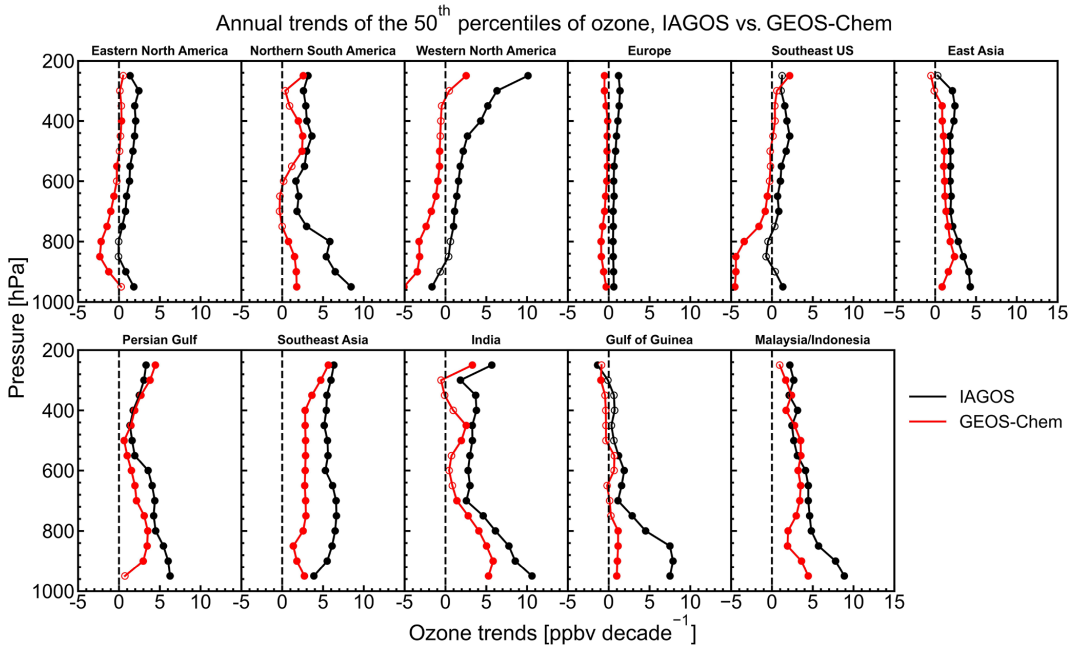

Figure 5. Annual trends of the 50th percentiles of IAGOS observed and GEOS-Chem simulated ozone (ppbv per decade) at intervals of 50 hPa. The trends are calculated between 1995 and 2017 above the 11 selected regions (Fig. 1) using the quantile regression method (Sect. 2.5). Filled circles indicate trends with $p < 0.05$.

method as described in Sect. 2.5. IAGOS observations show that the 50th percentile of tropospheric ozone has increased over all 11 study regions in the Northern Hemisphere in 1995–2017, as also pointed out by Gaudel et al. (2020). Large ozone increases are found from IAGOS observations in the lower troposphere (950–800 hPa) for all seasons over developing regions in the northern tropics and subtropics, including East Asia, Southeast Asia, the Persian Gulf, India, northern South America, the Gulf of Guinea, and Malaysia/Indonesia, with annual trends ranging from 2.8 to 10.6 ppbv per

decade. The observed 95th percentiles of lower-tropospheric ozone over these regions have increased by 3.6–24.2 ppbv per decade (Fig. S3), showing that the extreme ozone values are rising even faster. The positive trends extend to the free troposphere but with much smaller values. In comparison, the lower-tropospheric trends of the 50th percentile ozone in developed regions (Europe, North America) over the northern mid-latitudes are much smaller by up to 1.8 ppbv per decade, which is largely driven by boreal autumn and winter with $\sim$ 1.2 ppbv per decade on average (Fig. S4). There are small negative trends in the annual 50th percentile in the lower troposphere above North America driven by ozone decreases in the summer (Fig. S4) (Cooper et al., 2012; Simon et al., 2015; Gaudel et al., 2020). The annual 95th percentile in the lower troposphere above Europe and North America has declined at a rate of -0.4 to -8.3 ppbv per decade, which is consistent with surface ozone trends (Chang et al., 2017; Gaudel et al., 2018).

Figure 6 presents the vertical distributions of tropospheric ozone trends derived from ozonesonde observations, complementing ozone trend analyses from IAGOS by providing tropospheric ozone trends in remote regions and latitudes. We find the largest tropospheric ozone trends at the 50th percentile at three stations in the East Asia region, ranging from 3.8 to 6.7 ppbv per decade throughout the troposphere. Ozone at these stations is affected by the outflow of Asian pollution plumes, and tropospheric ozone trends there are even larger than those over the source region estimated from IAGOS observations. Notable ozone increases are also found at two stations in the southern subtropics, La Réunion and Natal, with 0.04–6.1 ppbv per decade in the middle troposphere and 4.6–9.3 ppbv per decade in the upper troposphere, in agreement with the results of Witte et al. (2017). At stations with higher latitudes, tropospheric ozone trends are generally smaller, and signs are varied among sites. As discussed in detail by Chang et al. (2020, 2022), low sampling frequencies at ozonesonde stations can make it difficult to detect a trend, and therefore discrepancies in trends from ozonesonde measurements in the free troposphere above Europe and western North America are not unexpected. When the sample size above these regions is maximized by combining all available ozonesonde and IAGOS profiles, the resulting combined product reveals increasing ozone above these regions from 1994 to 2019 (Chang et al., 2022).

We integrate in Fig. 7a and Table 4 the annual trends in median ozone for the tropospheric column (950–250 hPa) in 1995–2017 from both IAGOS and ozonesonde observations. This allows us to provide a more complete picture of observed global tropospheric ozone trends than previous studies focusing on the Northern Hemisphere alone (Gaudel et al., 2020) and to check the consistency between the two sources of ozone trend measurements. Both observational datasets consistently reveal widespread ozone increases in the troposphere over the past 2 decades, with larger ozone increases over developing regions in low latitudes than those over mid-latitudes and high latitudes. All 11 IAGOS areas and 19 of 27 ozonesonde sites have measured increases in tropospheric ozone by 2.9 ± 1.7 and 1.9 ± 1.7 ppbv per decade on average, respectively. In particular, trends in the northern low latitudes (0–30° N) are 4.2 and 2.4 ppbv per decade for ozone at the 50th percentile, averaged over all six IAGOS areas and three ozonesonde observations, respectively. In Europe and North America, observed trends are mostly positive, while three sites (Payerne, Legionowo, and Boulder) show inconsistently negative trends of -0.5 to -0.6 ppbv per decade that are in contrast to IAGOS observations (0.8–1.7 ppbv per decade) and trends at the other nearby sites (0.3–2.1 ppbv per decade). Increasing the sampling frequency (i.e., to 18 profiles per month according to Chang et al., 2020) would be helpful to reconcile the ozone trend estimate at adjacent ozonesonde sties, but we do not exclude the possibility that tropospheric ozone trends can still be variable even at adjacent locations. IAGOS observations provide less information in the Southern Hemisphere. Six of nine ozonesonde stations in the Southern Hemisphere show increasing tropospheric ozone, with the largest trends at low-latitudes sites in La Réunion and Natal (4.6 and 3.0 ppbv per decade; $p < 0.01$), while ozone in the southern mid-latitudes and high latitudes displays no significant tropospheric ozone trends in 1995–2017, with slight decreasing trends at two sites in Australia (Macquarie Island and Broadmeadows) and one site in Antarctica (Marambio).

Figures 5–7 and Table 4 also evaluate the performance of GEOS-Chem in reproducing the observed tropospheric ozone trends from IAGOS and ozonesondes. Our BASE simulation reproduces the overall pattern of tropospheric ozone trends in 1995–2017, in particular the larger ozone increases over the low latitudes, with a correlation coefficient $r = 0.6$ for all pairs of observed and simulated tropospheric ozone trends. GEOS-Chem simulated trends in tropospheric ozone are 2.1–2.9 ppbv per decade over East Asia, India, Southeast Asia, the Persian Gulf, and Malaysia/Indonesia, accounting for 51.8 %–81.4 % of the IAGOS trends over these rapidly developing regions (Table 4). We find a larger underestimation of ozone trends in the lower troposphere (950–800 hPa) compared to higher altitudes (Fig. 5). The model also catches the positive tropospheric ozone trends at three ozonesonde stations in East Asia of 0.5–1.8 ppbv per decade but are underestimated compared to the observed trends of 3.7–5.2 ppbv per decade. As discussed in Sect. 3.1, bias in anthropogenic emissions of ozone precursors during the early years of 1995–2017 over these developing regions may contribute to the underestimation of trends. The larger underestimation of tropospheric ozone trends over the Asian–Pacific ozonesonde sites may result from the coarse resolution of our simulation which is not adequate to resolve the Asian pollution outflow (Eastham and Jacob, 2017). In the northern middle and high latitudes (Europe and North America), GEOS-Chem estimates weak tropospheric ozone trends of -2.0 to 1.6 ppbv per decade at IAGOS regions and

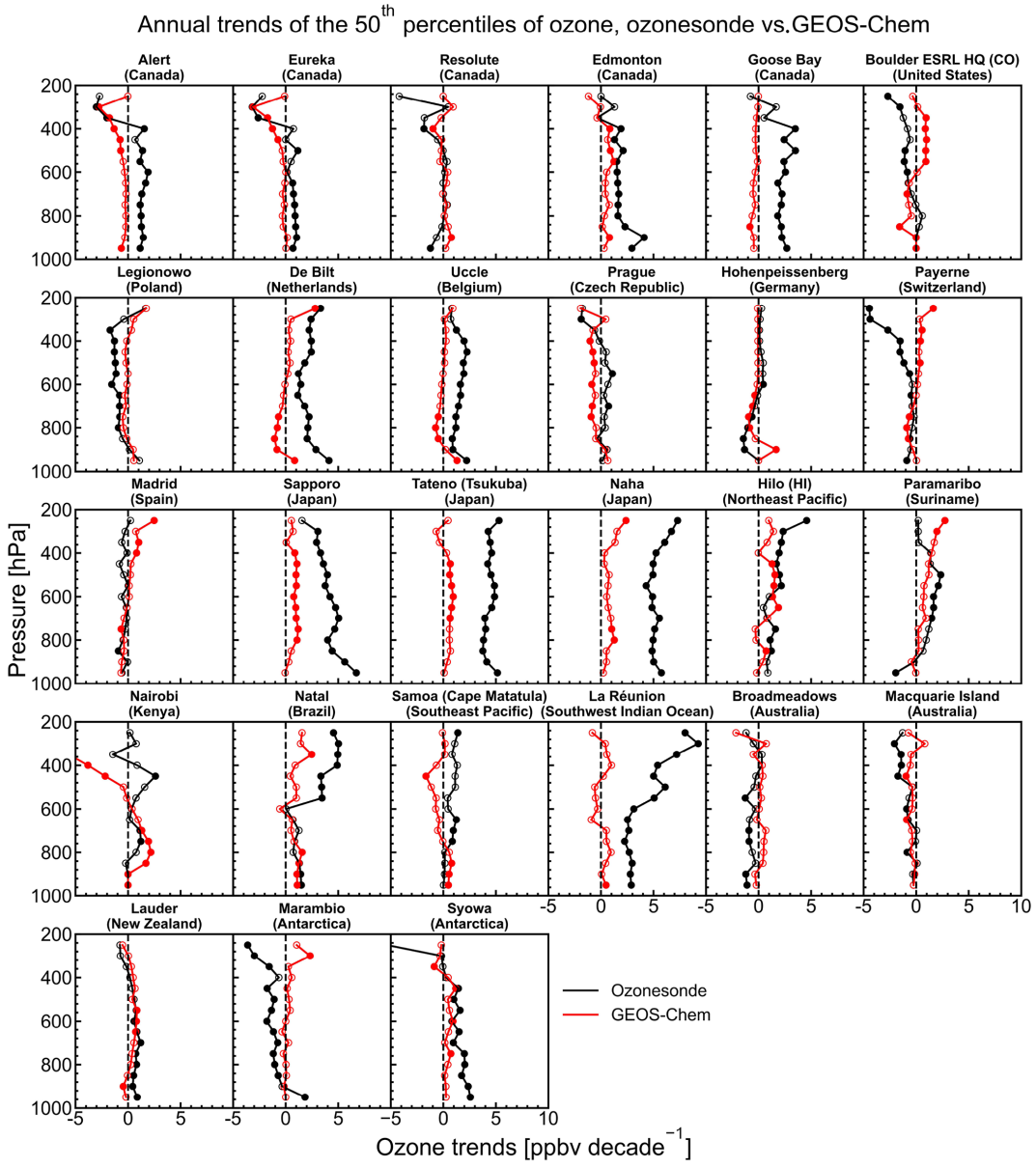

Figure 6. Same as Fig. 5 but for the comparison of ozonesonde vs. GEOS-Chem results.

ozonesonde stations, smaller than the spread of observed tropospheric ozone trends, reflecting the model difficulty in capturing weak and variable tropospheric ozone trends there. The model reproduces the ozone increases in the southern low latitudes (0.14–0.94 ppbv per decade, compared to 1.7–4.6 ppbv per decade from ozonesonde observations) except for Samoa and the varied tropospheric ozone trends over the southern mid-latitudes and high latitudes.

We compare the tropospheric ozone burden and trends in GEOS-Chem with the selected CMIP6 chemical models in Fig. 8. Here our GEOS-Chem simulation serves as a platform to evaluate tropospheric ozone trends in CMIP6 models, as the monthly mean output of CMIP6 models hinders a direct comparison against IAGOS and ozonesonde observations. GEOS-Chem estimates a global tropospheric ozone burden of 304.9 Tg averaged over 1995–2014 and 311.1 Tg for the year 2010, at the low end of the eight CMIP6 models for 1995–2014 (308.1–347.5 Tg) and the IPCC AR6 multi-model ensemble and observational estimates for 2010 (347 ± 28 Tg) (Szopa et al., 2021), again reflecting the low ozone bias in current GEOS-Chem versions (Christiansen et al., 2022) and the lower emissions in our simulations than CMIP6 simulations (Fig. 2). The interannual variability in tropospheric ozone burden in GEOS-Chem is moderately consistent with the CMIP6 models with r ranging from 0.3–0.6 (Fig. 8a).

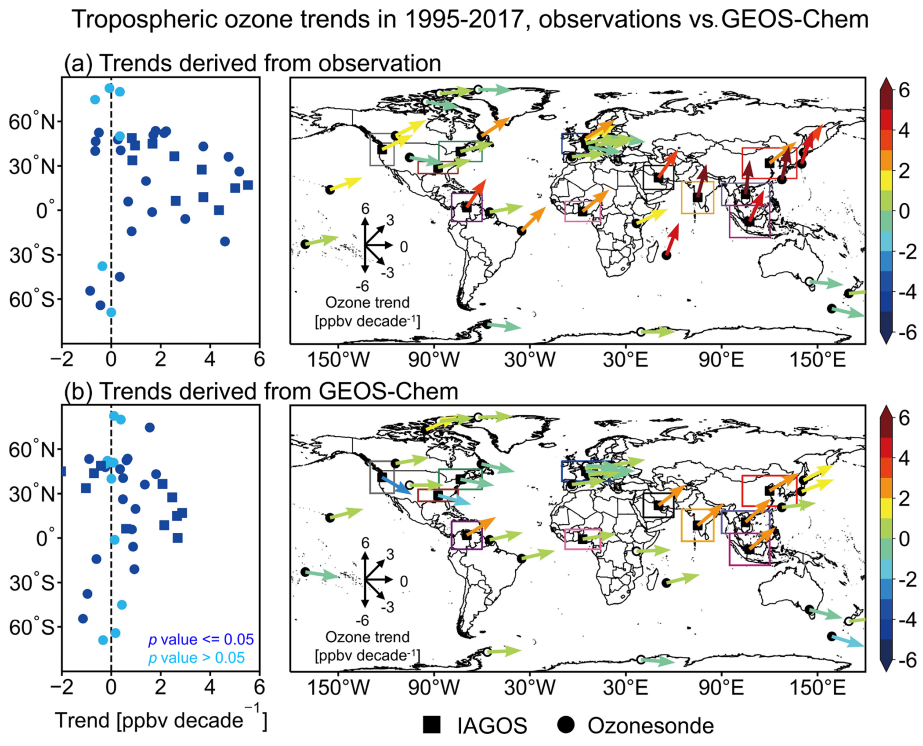

Figure 7. Comparison of tropospheric ozone trends of the 50th percentiles of the tropospheric column (950 to 250 hPa) in 1995–2017 derived from **(a)** observation and **(b)** GEOS-Chem. Trends are estimated for 11 selected IAGOS regions and ozonesonde sites with frequent sampling. Symbol colors indicate the p value associated with the trend at each site and region in the left panel. Both directions and colors of the vectors in the right panel indicate the ozone change rates (ppbv per decade). Dark colors (left panel) and filled circles or squares (right panel) indicated trends with $p < 0.05$.

All models show an increase in tropospheric ozone burden over the period 1995–2014, but the magnitude of trends differs by a factor of 4. GEOS-Chem estimates an increasing trend in global tropospheric ozone burden of 0.2 Tg yr^{-1}, which enlarges to 0.4 Tg yr^{-1} if 2015–2017 trends are included, but is still in the low end of the CMIP6 model ensemble (0.4 to 1.3 Tg yr^{-1}). We find in Figs. 8b and S5–S6 that all models agree with the significant ozone increases in 30° S–30° N, with tropospheric ozone burden increased by 2.4 % in 2010–2014 (3.7 % in 2013–2017) relative to 1995–1999 in GEOS-Chem and by 2.2 %–8.0 % in CMIP6 models, though the GEOS-Chem trends over 30° S–30° N are very likely underestimated compared to the observed trends as discussed above. However, GEOS-Chem simulation shows no notable ozone changes integrated in the 90–45° S and 45–90° N latitude bands, while a number of CMIP6 models show distinguished ozone increases. Our analyses of the observed tropospheric ozone trends from the IAGOS and ozonesonde observations in Fig. 7 suggest some inconsistency in tropospheric ozone trends poleward over 45° in the both hemispheres, indicating that the simulated ozone increases over these regions from some CMIP6 models need to be interpreted with caution. The weaker tropospheric ozone trends in our GEOS-Chem simulation compared to the CMIP6 models should mostly come from the smaller trends in global anthropogenic emissions in CEDSv2 compared to the CEDS$_{\mathrm{CMIP6}}$ inventory, as discussed in Sect. 2.3, but may also reflect the differences in driven meteorology or model mechanism. Global tropospheric ozone seasonal trends and drivers will be discussed in the next section.

3.3 Factors contributing to the tropospheric ozone trend and burden increase from 1995 to 2017

We now examine the factors contributing to tropospheric ozone trends from 1995 to 2017 from GEOS-Chem sensitivity simulations. Figure 9 summarizes the contribution to tropospheric ozone burden trends. Figures 10–11 present the seasonal mean distributions of tropospheric ozone trends and contributions from different drivers, separating anthropogenic and climatic/stratospheric influences as described in Sect. 2.3. Figure S7 presents the ozone trends and attributions at the surface level.

We find that changes in global anthropogenic emissions, including surface emissions of short-lived ozone precursors, methane, and aircraft emissions, are the main drivers of the increase in global tropospheric ozone burden and largely determine the overall spatial pattern of ozone trends in the BASE simulation in 1995–2017. Changes in anthro-

Table 4. Annual trends and 2σ uncertainty (ppbv per decade) in median ozone for the tropospheric column (950–250 hPa) in 1995–2017 from both observations and GEOS-Chem.

Region	Measurements	Ozonesonde site or IAGOS region	Observation		GEOS-Chem	
			Trend $\pm 2\sigma$	p value	Trend $\pm 2\sigma$	p value
East Asia	Ozonesonde	Sapporo	3.73 ± 0.69	< 0.01	1.82 ± 0.50	< 0.01
	Ozonesonde	Tateno (Tsukuba)	4.75 ± 0.43	< 0.01	1.36 ± 0.40	< 0.01
	Ozonesonde	Naha	5.18 ± 0.40	< 0.01	0.47 ± 0.41	< 0.05
	IAGOS	East Asia	2.55 ± 0.15	< 0.01	2.08 ± 0.17	< 0.01
India	IAGOS	India	5.01 ± 0.43	< 0.01	2.66 ± 0.36	< 0.01
Southeast Asia	IAGOS	Southeast Asia	5.53 ± 0.26	< 0.01	2.87 ± 0.23	< 0.01
Persian Gulf	IAGOS	Persian Gulf	3.66 ± 0.26	< 0.01	2.47 ± 0.19	< 0.01
Malaysia/Indonesia	IAGOS	Malaysia/Indonesia	4.36 ± 0.41	< 0.01	2.69 ± 0.33	< 0.01
Africa	IAGOS	Gulf of Guinea	2.61 ± 0.34	< 0.01	0.60 ± 0.27	< 0.01
	Ozonesonde	Nairobi	1.66 ± 0.56	< 0.01	0.14 ± 0.51	0.59
South America	Ozonesonde	Paramaribo	0.69 ± 0.63	< 0.05	0.84 ± 0.55	< 0.01
	Ozonesonde	Natal	3.00 ± 0.74	< 0.01	0.89 ± 0.75	< 0.05
	IAGOS	Northern South America	3.72 ± 0.50	< 0.01	2.14 ± 0.56	< 0.01
Pacific	Ozonesonde	Hilo (HI)	1.41 ± 0.46	< 0.01	0.98 ± 0.46	< 0.01
	Ozonesonde	Samoa (Cape Matatula)	0.83 ± 0.36	0.25	-0.60 ± 0.38	< 0.01
Europe	Ozonesonde	Legionowo	-0.50 ± 0.42	< 0.05	0.62 ± 0.35	< 0.01
	Ozonesonde	De Bilt	2.14 ± 0.37	< 0.01	-0.15 ± 0.34	0.38
	Ozonesonde	Uccle	1.70 ± 0.23	< 0.01	0.10 ± 0.20	0.34
	Ozonesonde	Prague	0.35 ± 0.43	0.11	-0.22 ± 0.46	0.33
	Ozonesonde	Hohenpeissenberg	0.27 ± 0.23	< 0.05	-0.24 ± 0.21	< 0.05
	Ozonesonde	Payerne	-0.63 ± 0.23	< 0.01	0.36 ± 0.19	< 0.01
	Ozonesonde	Madrid	0.38 ± 0.39	< 0.05	0.48 ± 0.36	< 0.01
	IAGOS	Europe	0.83 ± 0.06	< 0.01	-0.41 ± 0.05	< 0.01
United States	Ozonesonde	Boulder ESRL HQ (CO)	-0.64 ± 0.34	< 0.01	0.009 ± 0.35	0.96
	IAGOS	Eastern North America	0.96 ± 0.13	< 0.01	-0.70 ± 0.12	< 0.01
	IAGOS	Southeast US	0.86 ± 0.22	< 0.01	-1.02 ± 0.16	< 0.01
	IAGOS	Western North America	1.67 ± 0.32	< 0.01	-2.03 ± 0.37	< 0.01
Canada	Ozonesonde	Alert	-0.07 ± 1.22	0.91	0.11 ± 1.34	0.87
	Ozonesonde	Eureka	0.35 ± 1.13	0.53	0.39 ± 1.22	0.52
	Ozonesonde	Resolute	-0.65 ± 1.91	0.49	1.56 ± 1.37	< 0.05
	Ozonesonde	Edmonton	1.80 ± 0.57	< 0.01	0.66 ± 0.61	< 0.05
	Ozonesonde	Goose Bay	2.22 ± 0.74	< 0.01	-0.89 ± 0.63	< 0.01
Southern Hemisphere	Ozonesonde	La Réunion	4.60 ± 0.93	< 0.01	0.94 ± 0.95	< 0.05
	Ozonesonde	Broadmeadows	-0.36 ± 0.52	0.17	-0.96 ± 0.72	< 0.01
	Ozonesonde	Macquarie Island	-0.85 ± 0.43	< 0.01	-1.14 ± 0.76	< 0.01
	Ozonesonde	Lauder	0.34 ± 0.30	< 0.05	0.43 ± 0.51	0.09
	Ozonesonde	Marambio	-0.43 ± 0.36	< 0.05	0.17 ± 0.71	0.62
	Ozonesonde	Syowa	0.003 ± 0.37	0.99	-0.33 ± 0.54	0.22

pogenic emissions alone increase tropospheric ozone burden by $0.5\,\mathrm{Tg\,yr^{-1}}$ ($p < 0.01$), compared to the total simulated tropospheric ozone burden trend ($0.4\,\mathrm{Tg\,yr^{-1}}$; $p < 0.05$) in 1995–2017 (Fig. 9). The emission-driven increases are particularly large (1.0 ppbv per decade) in the northern low latitudes where we have observed the most notable ozone increases (Figs. 10–11). We have shown in Fig. 2 that the global anthropogenic emissions of NO_x and NMVOC emissions have been increasing and shifting equatorward from developed regions in the northern mid-latitudes in Europe and North America to the low latitudes from 1995 to 2017; in particular anthropogenic emissions of NO_x and NMVOCs have

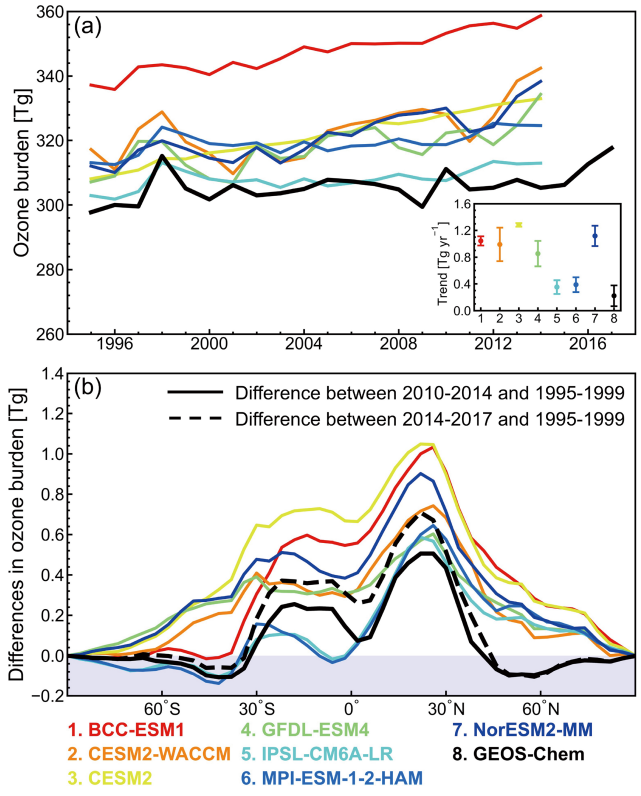

Figure 8. Evolution of 1995–2017 tropospheric ozone burden from GEOS-Chem and seven CMIP6 models (available for 1995–2014) used in this study. **(a)** The time series of tropospheric ozone burden integrated from 90° S to 90° N for the period 1995 to 2017. The black line represents the results of the GEOS-Chem simulation, and colored lines are from CMIP6 models. Dot plots show the tropospheric ozone burden trends for 1995–2014 in different models with the vertical bars showing the 95 % confidence interval. **(b)** The differences in zonal integrated tropospheric ozone burden for the nine models between 2010–2014 and 1995–1999 (solid line) and for GEOS-Chem between 2014–2017 and 1995–1999 (dashed line).

increased by 55.5 % and 35.6 %, respectively, in the 0–30° N latitudinal band. Emissions of ozone precursors at low latitudes produce ozone at high efficiency due to the higher solar radiation, temperature, and NO_x sensitivity compared to those at high latitudes (Zhang et al., 2016, 2021). Frequent deep convection at low latitudes also effectively lofts the pollutants to the upper troposphere and can further influence global tropospheric ozone trends via atmospheric circulation (Lawrence et al., 2003; Lu et al., 2019b). This is supported by the extended positive emission-driven ozone trends from the surface to upper troposphere over 0–30° N (Fig. 10). Our result highlights the significant role of the emission-driven ozone increases in tropospheric ozone trends since 1995.

Changes in anthropogenic emissions contribute to tropospheric ozone increases in 30–90° N in spring, autumn, and winter but lead to ozone decreases in summer (Fig. 10). This pattern reflects the differences in emission-driven tropospheric ozone trends between East Asia (positive) and Europe and the US (negative) (Fig. 11). The CEDSv2 emission inventory (Fig. 2) has documented rapid increases in anthropogenic emissions of ozone precursors over China, which contributed to significant increases in tropospheric ozone between 1995 and 2017 by about 2 ppbv per decade for all seasons. We find that at the surface changes in the anthropogenic emissions alone lead to larger ozone increases in summer by 5 ppbv per decade (Fig. S7) but decrease in surface ozone by −4 ppbv per decade in northern China in winter due to NO_x titration effect. However, we note that these surface trends are estimated from the coarse-resolution simulation at $4° \times 5°$. The emission-driven reduction in summertime ozone (and increases in wintertime ozone) over Europe and North America in 1995–2017 are clearly linked to the decline in anthropogenic NO_x emissions as documented in the literature (Cooper et al., 2012; Simon et al., 2015; Lin et al., 2017; Gaudel et al., 2018; Yan et al., 2018).

Anthropogenic emissions also increase tropospheric ozone in the Southern Hemisphere by 0.5 ppbv per decade. Estimates from the CEDSv2 emission inventory in the Southern Hemisphere show that anthropogenic emissions of CO, NO_x, and NMVOCs increased by 26.5 %–59.8 % from 1995 to 2017. In addition, emission-driven ozone increases in the tropics would also extend to the Southern Hemisphere through meridional atmospheric circulation.

We highlight here the disproportionately large but previously underappreciated contribution of aircraft emissions to 1995–2017 tropospheric ozone trends. Our FixAircraft simulation allows us to separate the impact of aircraft emissions alone from the total anthropogenic emissions on ozone trends. As mentioned in Sect. 2.2, aircraft NO_x emissions have increased by 76.2 % from 1995 but still only account for 3.3 % of the total anthropogenic NO_x emissions for the year 2017. However, they contribute to a global tropospheric burden trend of 0.3 Tg yr^{-1} ($p < 0.01$), accounting for 66 % of the total emission-driven tropospheric ozone trends (Fig. 9b). This disproportionately large contribution is because aircraft NO_x emissions are mainly released in the middle and upper troposphere, where the NO / NO_2 ratio is high and the lifetime of NO_x is long (Silvern et al., 2018), leading to a much higher ozone production efficiency compared to NO_x emissions at the surface. We find that aircraft emission-driven trends are higher in the Northern Hemisphere than the Southern Hemisphere due to the greater density of flights; higher in December–January–February than in June–July–August because of the longer lifetime of ozone and the lower NO_x levels in the free troposphere (as lightning NO_x emissions are lower in boreal winter); and higher in the upper troposphere, where (Fig. 10) tropospheric ozone has the largest radiative impacts.

Climatic factors (including stratospheric influences and natural emissions, as diagnosed from the FixAC simulation) contribute little to the trend of the global tropospheric ozone burden (−0.1 Tg yr^{-1}; $p = 0.3$) but have significant influ-

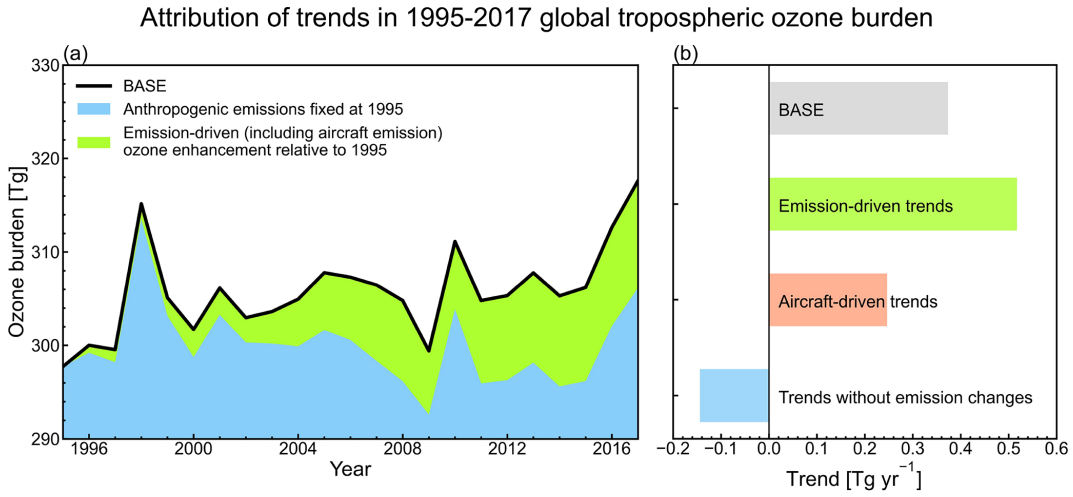

Figure 9. Drivers of global tropospheric ozone burden and trends from 1995 to 2017 estimated in the GEOS-Chem model. **(a)** Evolution of the GEOS-Chem simulated annual global tropospheric ozone burden (black line, same as Fig. 8a) in the BASE simulation. The blue shadings show the evolution of tropospheric ozone burden from the FixAC simulation, estimating ozone burden if anthropogenic emissions (surface emissions, aircraft emissions, and methane) are fixed at the level of 1995. The green shadings thus estimate the tropospheric ozone burden contributed by the anthropogenic emission (including aircraft emission) changes relative to the 1995 level. **(b)** The estimated tropospheric ozone trends from the BASE simulation and from different drivers.

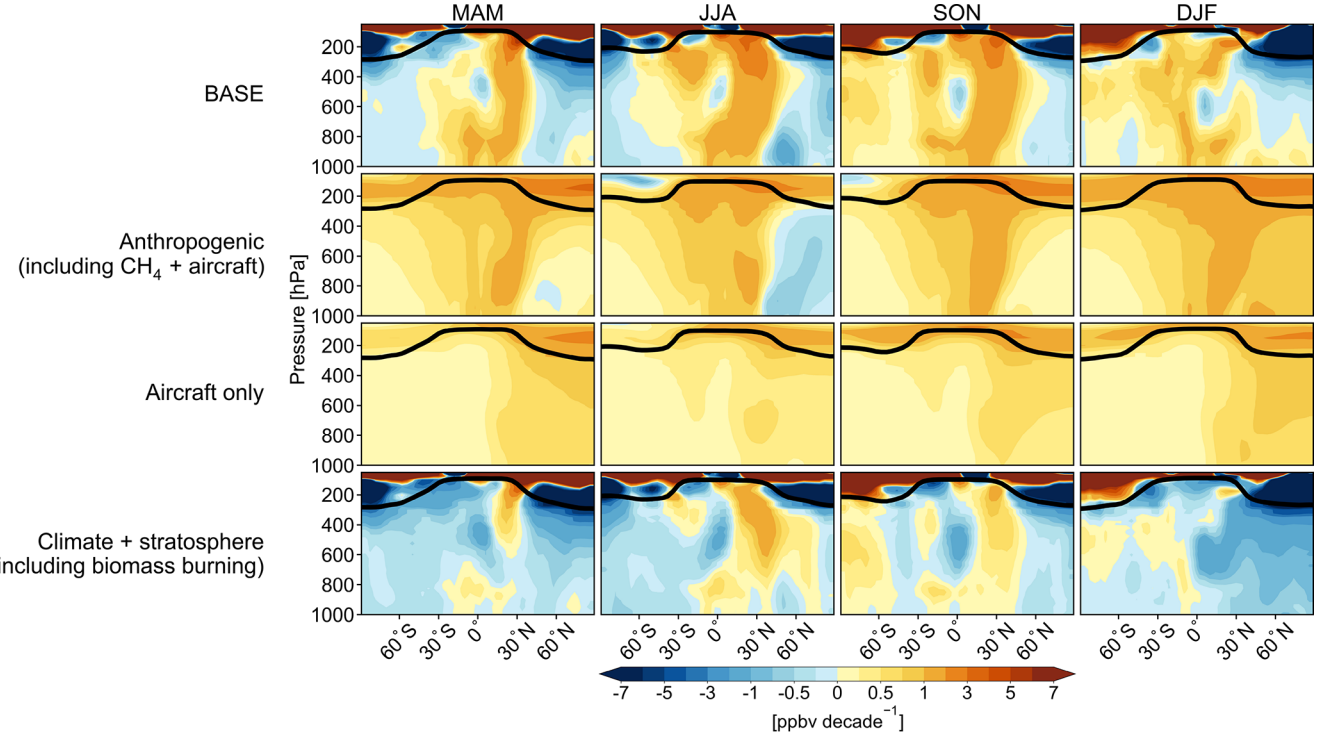

Figure 10. Drivers of seasonal zonal-mean ozone trends from 1995 to 2017 estimated in the GEOS-Chem model. Trends contributed by changes in anthropogenic emissions (surface emissions, aircraft emissions, and methane), aircraft emissions alone, and climatic and stratospheric factors are estimated. Black lines represent the 1995–2017 climatological seasonal mean tropopause from the MERRA-2 reanalysis dataset. MAM: March–April–May, JJA: June–July–August, SON: September–October–November, DJF: December–January–February.

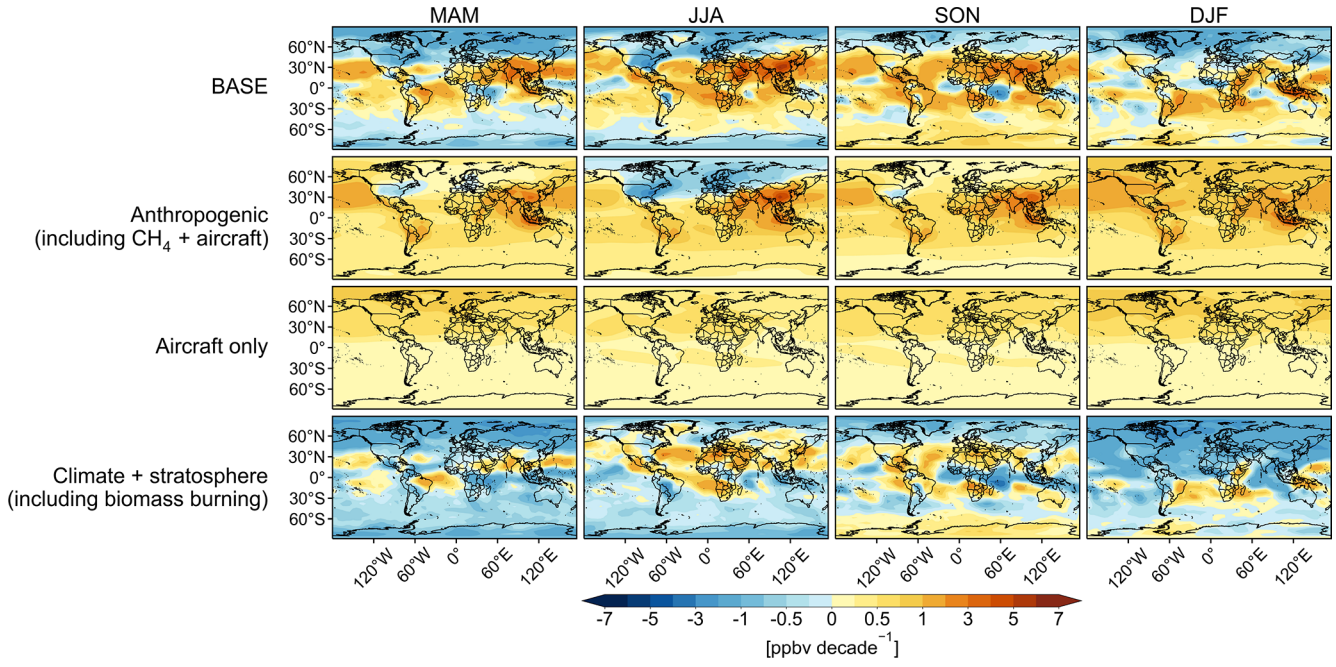

Figure 11. Drivers of seasonal mean tropospheric ozone (950–250 hPa) trends from 1995 to 2017 estimated in GEOS-Chem model. Trends contributed by changes in anthropogenic emissions (surface emissions, aircraft emissions, and methane), aircraft emissions alone, and climatic and stratospheric factors are estimated.

ence on its interannual variability. We find a high tropospheric ozone burden in 1998 and 2010 in GEOS-Chem and also in CMIP6 models. The high tropospheric ozone burden in these years is tied to the El Niño–Southern Oscillation (ENSO). ENSO influences global tropospheric ozone burden by modulating fire and lightning emissions and STE flux and influences regional ozone by modulating the transport pattern and local weather relevant to the ozone photochemical environment (Zeng and Pyle, 2005; Lin et al., 2014; Lu et al., 2019a). In particular, biomass burning emissions of CO are 36.4 % higher in 1998 (618.7 Tg) compared to 365.5 Tg averaged over 1995–2017, and we find that the anomalously high biomass burning emissions alone enhanced the tropospheric ozone burden by 7.8 Tg compared to a sensitivity simulation with fire activity fixed at the 1995 level. This is because the positive phase of ENSO (El Niño) in 1998 induces anomalous downward motion of air, which leads to hot and dry weather conditions over equatorial Asia and Central America and South America that are favorable for strong fire activity (Doherty et al., 2006; van der Werf et al., 2008; Fonseca et al., 2017). This El Niño-driven ozone peak in 1998 is more prominent in GEOS-Chem than most of the CMIP6 models, very likely because El Niño-driven shift in weather conditions and transport pattern is better reflected in MERRA-2 reanalysis data used to drive our GEOS-Chem model compared to climate fields simulated by CMIP6 climate–chemistry models without nudging to observed sea-surface temperature.

Figures 10–11 show that tropospheric ozone would decrease over mid-latitudes and high latitudes of both hemispheres in the absence of anthropogenic emission changes in 1995–2017, as estimated from the FixAC simulation. We find significant ozone decreases in the lower stratosphere in the Southern Hemisphere in March–August and in the Northern Hemisphere for all seasons, and the negative ozone trends extend downward to the troposphere (Fig. 10), indicating that changes in stratospheric ozone and/or stratosphere–troposphere dynamics are contributing to tropospheric ozone decreases. The ozone decreases in the lower stratosphere are inconsistent among the CMIP6 models (Fig. S5). Our GEOS-Chem model by implementing the time-resolved surface concentrations of ozone-depleting species as boundary conditions shows a moderate increasing trend in total stratospheric ozone burden from 1995 to 2017 (Fig. S8), consistent with the observations suggesting a leveling off of declining trends in stratospheric ozone after the Montreal Protocol (Solomon et al., 2016; Weber et al., 2022) and with other modeling studies (Griffiths et al., 2020). However, satellite observations have revealed that ozone in the lower stratosphere is still decreasing after the 1990s, and the drivers are still not clear (Ball et al., 2020), supporting the negative ozone trends in the lower stratosphere in GEOS-Chem.

We further use two methods to diagnose the STE flux in GEOS-Chem and examine their trends in 1995–2017. The first method diagnoses STE flux as a residual burden of ozone, calculated as STE = O_3 loss + O_3 dry depo-

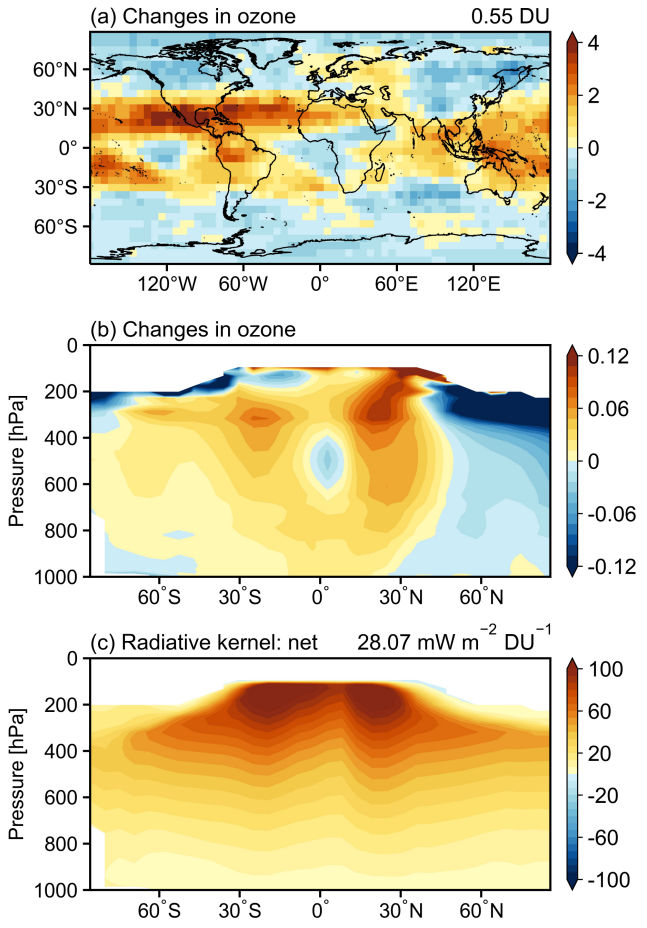

Figure 12. Changes in **(a)** annual mean tropospheric column ozone and **(b)** zonal-mean ozone between 2013–2017 and 1995–1999. **(c)** The values of the ozone radiative kernel (mW m^{-2} DU^{-1}) for net forcing (LW + SW) from Skeie et al. (2020). The values of the annual global mean are shown in the upper right.

sition − O_3 production + ΔO_3, where ΔO_3 is the change in tropospheric ozone burden relative to the previous year. This method is widely used in multi-model estimates of tropospheric ozone burden (Young et al., 2018; Archibald et al., 2020; Griffiths et al., 2020). The second method diagnoses the STE flux as the vertical ozone flux at 100 hPa (Hsu and Prather, 2014). As shown in Fig. S8, even though the absolute values of STE flux are not consistent between the two methods, both methods suggest a negative trend in STE flux in 1995–2017, consistent with a recent study using reanalysis data to diagnose long-term trend in STE flux (Wang and Fu, 2021). The decrease in STE flux explains the tropospheric ozone decreases over the high latitudes in the FixAC simulation. However, both methods are not applicable to derive STE trends at different latitude bands. More work is required to evaluate the trends in STE flux and to explore the driving factors.

3.4 Radiative impacts of tropospheric ozone changes in 1995–2017

We now examine the radiative impacts of tropospheric ozone changes in 1995–2017. Figure 12 shows the difference in modeled mean ozone in Dobson units (DU) between 2013–2017 and 1995–1999. We use the 5-year average for comparison to reduce the impact of short-term climate variability on ozone. Global average tropospheric column ozone increased by 0.6 DU in 2013–2017 compared to the 1995–1999 level, with the greatest increases in the tropics and in the upper troposphere (Fig. 12b), where ozone radiative impacts are the largest as reflected in the ozone radiative kernel (Figs. 12c and S9).

Figures 13a–c estimate the associated changes in radiative forcing for total radiation (SW + LW) and separately for SW and LW, using the ozone radiative-kernel method as described in Sect. 2.6. We find that the global averaged total tropospheric ozone radiative impact is 18.5 mW m^{-2} in 2013–2017 compared to 1995–1999 level, with 1.6 mW m^{-2} from the SW and 16.9 mW m^{-2} from the LW. This estimated radiative-impact value is approximately 4.7 % of the tropospheric ozone radiative forcing of 390 (270 to 510) mW m^{-2} in 2005–2014 relative to 1850 estimated from 10 climate models in CMIP6 using the same radiative-kernel method (Skeie et al., 2020). In comparison, changes in global anthropogenic NO_x emissions between 2017 and 1995 are 3.9 % (1.7 TgN) of those between 2014 and 1850 (43.2 TgN). However, as our model has underestimated tropospheric ozone trends, the calculated ozone-induced radiative impacts are very likely smaller than the true forcing. Peak SW radiative impact is found in regions with large ozone changes and high albedo, such as over deserts or ice, and with low clouds. The LW radiative impact peaks in areas with large ozone changes and with hot surface temperatures and high tropopause levels. Thus, we see large ozone radiative impact over the northern tropics.

Figure 13d–e further attribute the total tropospheric ozone radiative impacts to changes in anthropogenic emissions, aircraft emissions only, and climatic and stratospheric influences. Changes in anthropogenic emissions contribute to tropospheric ozone radiative impact by 43.5 mW m^{-2}, representing the dominant factor driving the increase in tropospheric ozone radiative impact from 1995. In particular, aircraft emissions alone contribute to tropospheric ozone radiative impact by 20.5 mW m^{-2}. The large emission-driven tropospheric ozone radiative-impact increases from 1995 to 2017 not only are due to the increase in the absolute amount of emissions but also reflect the equatorward redistribution of emissions to regions with strong convection and the increases in aircraft emissions, which have both led to ozone increases in the middle and upper troposphere and over the tropics, where the potential for tropospheric ozone radiative impacts are 1 or 2 orders of magnitude larger than those at the surface over mid-latitudes (Fig. 12c). Nevertheless, our analysis does

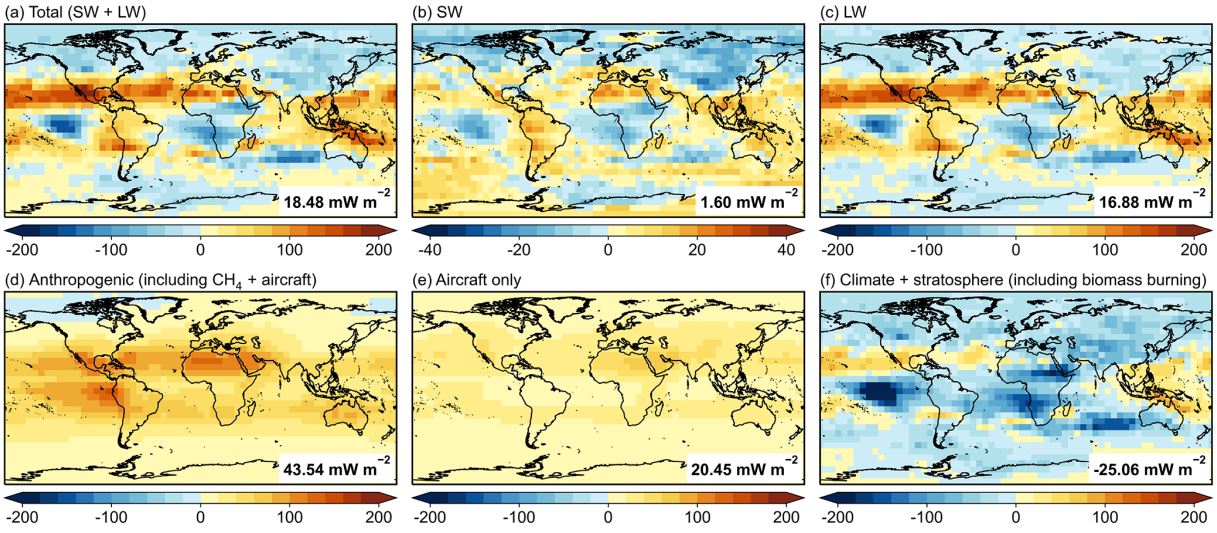

Figure 13. Tropospheric ozone radiative impacts and attributions for 2013–2017 vs. 1995–1999. **(a–c)** The tropospheric ozone radiative impacts (mW m^{-2}) for total (SW + LW) and for SW and LW, respectively. **(d–f)** Attribution of the tropospheric ozone radiative impacts due to changes in anthropogenic emissions (including surface emissions, aircraft emission, and global methane levels), aircraft emissions alone, and climate (including the stratosphere and biomass burning) between 2013–2017 and 1995–1999. The values of the annual global mean are shown inset.

not reflect the long-term indirect radiative impacts of aircraft emissions through modulating tropospheric OH and CH_4 and stratospheric chemistry (Lee et al., 2021). The climatic and stratospheric influences contribute -25.1 mW m^{-2} to tropospheric ozone radiative impact, mainly reflecting the simulated ozone decreases in the extratropical upper troposphere.

4 Conclusions

We examine the tropospheric ozone trends, their attributions, and radiative impact from 1995–2017 using aircraft (IAGOS) observations, ozonesondes, and a multi-decadal GEOS-Chem chemical model simulation. The combination of IAGOS and ozonesonde observations provides a global view of tropospheric ozone trends and enables an extensive evaluation of GEOS-Chem simulated tropospheric ozone trends. We attribute tropospheric ozone trends to changes in anthropogenic emissions and climatic and stratospheric factors through a set of GEOS-Chem sensitivity experiments and calculate the change in tropospheric ozone radiative forcing during 1995–2017.

We find that both the IAGOS and ozonesonde observations reveal significant tropospheric ozone increases over the tropics in 1995–2017. The largest positive ozone trends in the lower troposphere are found over developing regions (East Asia, the Persian Gulf, India, northern South America, the Gulf of Guinea, and Malaysia/Indonesia), ranging from 2.8 to 10.6 ppbv per decade for IAGOS and 3.8 to 6.7 ppbv per decade for ozonesondes in this period. In Europe and North America, however, we find much weaker tropospheric ozone trends and some inconsistency in the sign of tropospheric ozone trends derived from IAGOS and ozonesondes. Six ozonesonde stations in the Southern Hemisphere have increasing trends in free tropospheric ozone, with the strongest trends at the low-latitude sites of La Réunion and Natal. No significant tropospheric ozone increases are found at high latitudes in both hemispheres in 1995–2017.

Our GEOS-Chem simulation driven by reanalysis meteorological fields and the most up-to-date year-specific anthropogenic emission inventory reproduces the large tropospheric ozone increases over the tropics in 1995–2017. GEOS-Chem simulated trends in tropospheric ozone account for 51.8 %–81.4 % of the IAGOS trends over East Asia, India, Southeast Asia, the Persian Gulf, and Malaysia/Indonesia and also catch the positive tropospheric ozone trends at three ozonesonde stations in East Asia, but trends are largely underestimated. Comparisons of observed vs. modeled ozone values in 1995–1999 suggest that emissions in the early years in developing regions are likely overestimated and contribute to the underestimation of tropospheric ozone trends. In the northern middle and high latitudes, the model shows no notable tropospheric ozone trends. GEOS-Chem estimates an increasing trend in global tropospheric ozone burden of 0.2 Tg yr^{-1} in 1995–2014 (0.4 Tg yr^{-1} in 1995–2017), compared to the CMIP6 model ensemble of 0.4 to 1.3 Tg yr^{-1} in 1995–2014. The smaller tropospheric ozone trends in GEOS-Chem compared to most of the CMIP6 models are partly due to the smaller trends in anthropogenic emissions of ozone precursors in the CEDSv2 inventory than the $CEDS_{CMIP6}$ inventory used in the CMIP6 models and also because GEOS-Chem better captures the observed ozone decreases in the lower stratosphere.

We find that increases in the global anthropogenic emissions, including surface emissions of short-lived ozone precursors, aircraft emissions, and methane, contribute to increases in the tropospheric ozone burden by $0.5\,\mathrm{Tg\,yr^{-1}}$, acting as the dominant driver of the tropospheric ozone increase in 1995–2017. The larger emission-driven tropospheric ozone trends are found in the developing regions in the low latitudes, where emissions of ozone precursors can produce ozone at higher efficiency due to the higher solar radiation and NO_x sensitivity compared to those at high latitudes and can effectively influence the global ozone burden through deep convection. In particular, we find a previously underappreciated contribution of aircraft emissions to the tropospheric ozone increase ($0.3\,\mathrm{Tg\,yr^{-1}}$), accounting for 66 % of the total emission-driven tropospheric ozone trends. This large contribution is because aircraft NO_x emissions are mainly released in the mid-troposphere and upper troposphere, where water vapor content is lower, the NO_x level is low, and the lifetime of NO_x is longer, leading to higher ozone production efficiency. Climatic and stratospheric factors contribute to a reduction in tropospheric ozone over mid-latitudes and high latitudes of both hemispheres in the absence of anthropogenic emission changes in 1995–2017. Ozone decreases in the lower stratosphere and a negative trend in STE flux in 1995–2017 may explain this decrease in ozone at mid-latitudes and high latitudes. Climate variability such as ENSO largely influences the variability in tropospheric ozone through modulating biomass burning emissions.

We also examine the radiative impacts of tropospheric ozone changes in 1995–2017. We estimate a global mean tropospheric ozone total radiative impact of $18.5\,\mathrm{mW\,m^{-2}}$ in 2013–2017 compared to the 1995–1999 level, with an increase by ~ 1.2 %, but we suggest the true radiative impacts should be larger as our simulation underestimates the overall tropospheric ozone trends from 1995–2017. Changes in anthropogenic emissions are the dominant factor driving the increase in ozone radiative impact from 1995. The increase is mainly attributed to the equatorward redistribution of emissions to areas with strong convection and the increase in aircraft emissions; both contribute to the increase in ozone in the mid-troposphere and upper troposphere and over the tropics where the potential ozone radiative impacts are 1 or 2 orders of magnitude larger than those at the surface over mid-latitudes.

Our study thus highlights the dominant contribution of changes in global anthropogenic emission patterns, including the equatorward redistribution of surface emissions and the rapid increases in aircraft emissions, to the increases in tropospheric ozone and resulting radiative impacts in 1995–2017. Uncertainties in the anthropogenic emission inventory, especially for the early period and for developing regions where activity data are less effectively collected/constrained, may lead to the underestimation of GEOS-Chem simulated tropospheric ozone trends, especially in the tropics. Using long-term satellite observations of NO_x as a top-down constraint on trends in anthropogenic emissions (Qu et al., 2020; Chen et al., 2021) may help to improve the model's ability to capture observed ozone trends. The spatial resolution of $4° \times 5°$ in our simulations limits the model's ability to capture finer-scale ozone trends. We also call for more modeling studies to better understand ozone variability in the lower stratosphere and to quantify its impact on tropospheric ozone trends.

Data availability. The ozonesonde data are from https://woudc.org/data.php (World Ozone and Ultraviolet Radiation Data Centre, 2022). The IAGOS dataset is archived at http://www.iagos-data.fr/ (IAGOS, 2022). The updated global anthropogenic emissions data from CEDS are available from https://data.pnnl.gov/dataset/CEDS-4-21-21 (O'Rourke et al., 2021). The MERRA-2 reanalysis data are from http://geoschemdata.wustl.edu/ExtData/GEOS_4x5/MERRA2/ (GMAO, 2022). The CMIP6 model outputs are available on the Earth System Grid Federation (ESGF) website (https://esgf-data.dkrz.de/search/cmip6-dkrz/, Earth System Grid Federation, 2022). The tropopause pressure data from MERRA-2 are available at https://doi.org/10.5067/AP1B0BA5PD2K (Global Modeling and Assimilation Office, 2015). Data from GEOS-Chem modeling that support the findings of this study can be accessed by contacting the corresponding authors (Xiao Lu, luxiao25@mail.sysu.edu.cn; Shaojia Fan, eesfsj@mail.sysu.edu.cn).

Supplement. The supplement related to this article is available online at: https://doi.org/10.5194/acp-22-13753-2022-supplement.

Author contributions. XL, SJF, and HW designed the study. HW conducted the modeling and data analyses with contributions from BS and KW. DJJ, ORC, KLC, KL, MG, and YL advised regarding the trend analyses and model interpretation. TW and JZ contributed to the CMIP6 model result and its interpretation. BS, PN, and RB contributed the IAGOS data and advised on its interpretation. HW, XL, and SF wrote the paper with input from all authors. All authors contributed to the discussion and improvement of the paper.

Competing interests. The contact author has declared that none of the authors has any competing interests.

Disclaimer. Publisher's note: Copernicus Publications remains neutral with regard to jurisdictional claims in published maps and institutional affiliations.

Acknowledgements. The authors acknowledge the strong support of the European Commission, Airbus, and the airlines (Lufthansa, Air France, Austrian, Air Namibia, Cathay Pacific, Iberia, and China Airlines, so far) who have carried the MOZAIC (Measurements of Ozone on Airbus In-Service Aircraft) or IAGOS equipment and performed the maintenance since 1994. In its last 10 years of operation, MOZAIC has been funded by

INSU-CNRS (Institut national des sciences de l'Univers, Centre national de la recherche scientifique) (France), Météo-France, Université Toulouse III – Paul Sabatier (Toulouse, France), and Forschungszentrum Jülich (FZJ, Jülich, Germany). IAGOS has been additionally funded by the EU projects IAGOS-DS (Design Study) and IAGOS-ERI (European Research Infrastructure). The MOZAIC–IAGOS database is supported by AERIS, the French portal for data and service for the atmosphere. The data are available at https://www.iagos.org/ thanks to additional support from AERIS. Owen R. Cooper and Kai-Lan Chang were supported by a NOAA Cooperative Agreement with CIRES (Cooperative Institute for Research in Environmental Sciences; no. NA17OAR4320101). The authors thank David Lee, Ruijun Dang, Sebastian Eastham, and Viral Shah for valuable discussions on aircraft emissions.

Financial support. This research has been supported by the National Natural Science Foundation of China (NSFC; grant no. 42105103), Key-Area Research and Development Program of Guangdong Province (grant no. 2020B1111360003), Guangdong Major Project of Basic and Applied Basic Research (grant no. 2020B0301030004), Guangdong Science and Technology Plan Project (grant no. 2019B121201002), and Fundamental Research Funds for the Central Universities (Sun Yat-sen University; grant no. 22qntd1908).

Review statement. This paper was edited by Leiming Zhang and reviewed by two anonymous referees.

References

ADE: National Pollutant Inventory (NPI), http://www.npi.gov.au/substances (last access: 30 May 2022), 2016.

ADE: National Pollution Inventory, 2017/2018, http://www.npi.gov.au/npidata/action/load/advance-search (last access: 30 May 2022), 2019.

Amos, H. M., Jacob, D. J., Holmes, C. D., Fisher, J. A., Wang, Q., Yantosca, R. M., Corbitt, E. S., Galarneau, E., Rutter, A. P., Gustin, M. S., Steffen, A., Schauer, J. J., Graydon, J. A., Louis, V. L. St., Talbot, R. W., Edgerton, E. S., Zhang, Y., and Sunderland, E. M.: Gas-particle partitioning of atmospheric Hg(II) and its effect on global mercury deposition, Atmos. Chem. Phys., 12, 591–603, https://doi.org/10.5194/acp-12-591-2012, 2012.

Archibald, A. T., Folberth, G., Wade, D. C., and Scott, D.: A world avoided: impacts of changes in anthropogenic emissions on the burden and effects of air pollutants in Europe and North America, Faraday Discuss., 200, 475–500, https://doi.org/10.1039/C7FD00004A, 2017.

Archibald, A. T., Neu, J. L., Elshorbany, Y. F., Cooper, O. R., Young, P. J., Akiyoshi, H., Cox, R. A., Coyle, M., Derwent, R. G., Deushi, M., Finco, A., Frost, G. J., Galbally, I. E., Gerosa, G., Granier, C., Griffiths, P. T., Hossaini, R., Hu, L., Jöckel, P., Josse, B., Lin, M. Y., Mertens, M., Morgenstern, O., Naja, M., Naik, V., Oltmans, S., Plummer, D. A., Revell, L. E., Saiz-Lopez, A., Saxena, P., Shin, Y. M., Shahid, I., Shallcross, D., Tilmes, S., Trickl, T., Wallington, T. J., Wang, T., Worden, H. M., and Zeng, G.: Tropospheric Ozone Assessment Report: A critical review of changes in the tropospheric ozone burden and budget from 1850 to 2100, Elem. Sci. Anth., 8, 034, https://doi.org/10.1525/elementa.2020.034, 2020.

Atkinson, R.: Atmospheric chemistry of VOCs and NO_x, Atmos. Environ., 34, 2063–2101, https://doi.org/10.1016/S1352-2310(99)00460-4, 2000.

Ball, W. T., Chiodo, G., Abalos, M., Alsing, J., and Stenke, A.: Inconsistencies between chemistry–climate models and observed lower stratospheric ozone trends since 1998, Atmos. Chem. Phys., 20, 9737–9752, https://doi.org/10.5194/acp-20-9737-2020, 2020.

Bentsen, M., Oliviè, D. J. L., Seland, Ø., Toniazzo, T., Gjermundsen, A., Graff, L. S., Debernard, J. B., Gupta, A. K., He, Y., Kirkevåg, A., Schwinger, J., Tjiputra, J., Aas, K. S., Bethke, I., Fan, Y., Griesfeller, J., Grini, A., Guo, C., Ilicak, M., Karset, I. H. H., Landgren, O. A., Liakka, J., Moseid, K. O., Nummelin, A., Spensberger, C., Tang, H., Zhang, Z., Heinze, C., Iversen, T., and Schulz, M.: NCC NorESM2-MM model output prepared for CMIP6 CMIP historical, Earth System Grid Federation, https://doi.org/10.22033/ESGF/CMIP6.8040, 2019.

Bey, I., Jacob, D. J., Yantosca, R. M., Logan, J. A., Field, B. D., Fiore, A. M., Li, Q., Liu, H. Y., Mickley, L. J., and Schultz, M. G.: Global modeling of tropospheric chemistry with assimilated meteorology: Model description and evaluation, J. Geophys. Res.-Atmos., 106, 23073–23095, https://doi.org/10.1029/2001JD000807, 2001.

Bian, H. and Prather, M. J.: Fast-J2: Accurate Simulation of Stratospheric Photolysis in Global Chemical Models, J. Atmos. Chem., 41, 281–296, https://doi.org/10.1023/A:1014980619462, 2002.

Blot, R., Nedelec, P., Boulanger, D., Wolff, P., Sauvage, B., Cousin, J.-M., Athier, G., Zahn, A., Obersteiner, F., Scharffe, D., Petetin, H., Bennouna, Y., Clark, H., and Thouret, V.: Internal consistency of the IAGOS ozone and carbon monoxide measurements for the last 25 years, Atmos. Meas. Tech., 14, 3935–3951, https://doi.org/10.5194/amt-14-3935-2021, 2021.

Boucher, O., Denvil, S., Levavasseur, G., Cozic, A., Caubel, A., Foujols, M.-A., Meurdesoif, Y., Cadule, P., Devilliers, M., Ghattas, J., Lebas, N., Lurton, T., Mellul, L., Musat, I., Mignot, J., and Cheruy, F.: IPSL IPSL-CM6A-LR model output prepared for CMIP6 CMIP, Earth System Grid Federation [data set], https://doi.org/10.22033/ESGF/CMIP6.1534, 2018.

Chang, K.-L., Petropavlovskikh, I., Cooper, O. R., Schultz, M. G., and Wang, T.: Regional trend analysis of surface ozone observations from monitoring networks in eastern North America, Europe and East Asia, Elem. Sci. Anth., 5, 50, https://doi.org/10.1525/elementa.243, 2017.

Chang, K.-L., Schultz, M. G., Lan, X., McClure-Begley, A., Petropavlovskikh, I., Xu, X., and Ziemke, J. R.: Trend detection of atmospheric time series: Incorporating appropriate uncertainty estimates and handling extreme events, Elem. Sci. Anth., 9, 00035, https://doi.org/10.1525/elementa.2021.00035, 2021.

Chang, K.-L., Cooper, O. R., Gaudel, A., Allaart, M., Ancellet, G., Clark, H., Godin-Beekmann, S., Leblanc, T., Van Malderen, R., Nédélec, P., Petropavlovskikh, I., Steinbrecht, W., Stübi, R., Tarasick, D. W., and Torres, C.: Impact of the COVID-19 Economic Downturn on Tropospheric Ozone Trends: An Uncertainty Weighted Data Synthesis for Quantifying Regional Anomalies Above Western North America and Europe, AGU Adv., 3, e2021AV000542, https://doi.org/10.1029/2021AV000542, 2022.

Chang, K.-L., Cooper, O. R., Gaudel, A., Petropavlovskikh, I., and Thouret, V.: Statistical regularization for trend detection: an integrated approach for detecting long-term trends from sparse tropospheric ozone profiles, Atmos. Chem. Phys., 20, 9915–9938, https://doi.org/10.5194/acp-20-9915-2020, 2020.

Chen, Y., Zhang, L., Henze, D. K., Zhao, Y., Lu, X., Winiwarter, W., Guo, Y., Liu, X., Wen, Z., Pan, Y., and Song, Y.: Interannual variation of reactive nitrogen emissions and their impacts on $PM_{2.5}$ air pollution in China during 2005–2015, Environ. Res. Lett., 16, 125004, https://doi.org/10.1088/1748-9326/ac3695, 2021.

Christiansen, A., Mickley, L. J., Liu, J., Oman, L. D., and Hu, L.: Multidecadal increases in global tropospheric ozone derived from ozonesonde and surface site observations: Can models reproduce ozone trends?, Atmos. Chem. Phys. Discuss. [preprint], https://doi.org/10.5194/acp-2022-330, in review, 2022.

Cohen, Y., Petetin, H., Thouret, V., Marécal, V., Josse, B., Clark, H., Sauvage, B., Fontaine, A., Athier, G., Blot, R., Boulanger, D., Cousin, J.-M., and Nédélec, P.: Climatology and long-term evolution of ozone and carbon monoxide in the upper troposphere–lower stratosphere (UTLS) at northern midlatitudes, as seen by IAGOS from 1995 to 2013, Atmos. Chem. Phys., 18, 5415–5453, https://doi.org/10.5194/acp-18-5415-2018, 2018.

Cooper, O. R., Stohl, A., Hübler, G., Hsie, E. Y., Parrish, D. D., Tuck, A. F., Kiladis, G. N., Oltmans, S. J., Johnson, B. J., Shapiro, M., Moody, J. L., and Lefohn, A. S.: Direct transport of midlatitude stratospheric ozone into the lower troposphere and marine boundary layer of the tropical Pacific Ocean, J. Geophys. Res.-Atmos., 110, D23310, https://doi.org/10.1029/2005JD005783, 2005.

Cooper, O. R., Gao, R.-S., Tarasick, D., Leblanc, T., and Sweeney, C.: Long-term ozone trends at rural ozone monitoring sites across the United States, 1990–2010, J. Geophys. Res.-Atmos., 117, D22307, https://doi.org/10.1029/2012JD018261, 2012.

Cooper, O. R., Schultz, M. G., Schröder, S., Chang, K.-L., Gaudel, A., Benítez, G. C., Cuevas, E., Fröhlich, M., Galbally, I. E., Molloy, S., Kubistin, D., Lu, X., McClure-Begley, A., Nédélec, P., O'Brien, J., Oltmans, S. J., Petropavlovskikh, I., Ries, L., Senik, I., Sjöberg, K., Solberg, S., Spain, G. T., Spangl, W., Steinbacher, M., Tarasick, D., Thouret, V., and Xu, X.: Multi-decadal surface ozone trends at globally distributed remote locations, Elem. Sci. Anth., 8, 23, https://doi.org/10.1525/elementa.420, 2020.

Danabasoglu, G.: NCAR CESM2 model output prepared for CMIP6 CMIP historical, Earth System Grid Federation [data set], https://doi.org/10.22033/ESGF/CMIP6.7627, 2019a.

Danabasoglu, G.: NCAR CESM2-WACCM model output prepared for CMIP6 CMIP historical, Earth System Grid Federation [data set], https://doi.org/10.22033/ESGF/CMIP6.10071, 2019b.

Daniel, J. S., Velders, G. J. M., Douglass, A. R., Forster, P. M. D., Hauglustaine, D. A., Isaksen, I. S. A., Kuijpers, L. J. M., McCulloch, A., and Wallington, T. J.: Halocarbon scenarios, ozone depletion potentials, and global warming potentials (Chapter 8), in: Scientific Assessment of Ozone Depletion: 2006, World Meteorological Organization, Geneva, Switzerland, https://csl.noaa.gov/assessments/ozone/2006/chapters/chapter8.pdf (last access: 16 October 2022), 2007.

Doherty, R. M., Stevenson, D. S., Johnson, C. E., Collins, W. J., and Sanderson, M. G.: Tropospheric ozone and El Niño–Southern Oscillation: Influence of atmospheric dynamics, biomass burning emissions, and future climate change, J. Geophys. Res.-Atmos., 111, D19304, https://doi.org/10.1029/2005JD006849, 2006.

Earth System Grid Federation: The complete archive of World Climate Research Programme Coupled Model Intercomparison Project (Phase 6) output, Earth System Grid Federation [data set], https://esgf-node.llnl.gov/projects/cmip6/, last access: 16 October 2022.

Eastham, S. D., Weisenstein, D. K., and Barrett, S. R. H.: Development and evaluation of the unified tropospheric–stratospheric chemistry extension (UCX) for the global chemistry-transport model GEOS-Chem, Atmos. Environ., 89, 52–63, https://doi.org/10.1016/j.atmosenv.2014.02.001, 2014.

Eastham, S. D. and Jacob, D. J.: Limits on the ability of global Eulerian models to resolve intercontinental transport of chemical plumes, Atmos. Chem. Phys., 17, 2543–2553, https://doi.org/10.5194/acp-17-2543-2017, 2017.

ECCC: Air pollutant emissions inventory report: 1990–2014, http://www.ec.gc.ca/Pollution/A17452DA-CFC0-4222-985F-36B12FCBAA0B/APEI2017-E-Feb_15_2017.pdf (last access: 30 May 2022), 2016.

ECCC: Canada's 2019 Air Pollutant Emissions Inventory, http://data.ec.gc.ca/data/substances/monitor/canada-s-air-pollutant-emissions-inventory/APEI_Tables_Canada_Provinces_Territories/?lang (last access: 30 May 2022), 2019.

Edwards, J. M. and Slingo, A.: Studies with a flexible new radiation code. I: Choosing a configuration for a large-scale model, Q. J. Roy. Meteor. Soc., 122, 689–719, https://doi.org/10.1002/qj.49712253107, 1996.

EMEP: Officially reported emission data, http://www.ceip.at/ (last access: 30 May 2022), 2016.

EMEP: Officially reported emission data to the European Monitoring and Evaluation Programme: EMEP_NFR14_LEVEL1 data, https://www.ceip.at/ms/ceip_home1/ceip_home/webdab_emepdatabase/reported_emissiondata/ (last access: 30 May 2022), 2019.

Eyring, V., Bony, S., Meehl, G. A., Senior, C. A., Stevens, B., Stouffer, R. J., and Taylor, K. E.: Overview of the Coupled Model Intercomparison Project Phase 6 (CMIP6) experimental design and organization, Geosci. Model Dev., 9, 1937–1958, https://doi.org/10.5194/gmd-9-1937-2016, 2016.

Feng, L., Smith, S. J., Braun, C., Crippa, M., Gidden, M. J., Hoesly, R., Klimont, Z., van Marle, M., van den Berg, M., and van der Werf, G. R.: The generation of gridded emissions data for CMIP6, Geosci. Model Dev., 13, 461–482, https://doi.org/10.5194/gmd-13-461-2020, 2020.

Fischer, E. V., Jacob, D. J., Yantosca, R. M., Sulprizio, M. P., Millet, D. B., Mao, J., Paulot, F., Singh, H. B., Roiger, A., Ries, L., Talbot, R. W., Dzepina, K., and Pandey Deolal, S.: Atmospheric peroxyacetyl nitrate (PAN): a global budget and source attribution, Atmos. Chem. Phys., 14, 2679–2698, https://doi.org/10.5194/acp-14-2679-2014, 2014.

Fleming, Z. L., Doherty, R. M., von Schneidemesser, E., Malley, C. S., Cooper, O. R., Pinto, J. P., Colette, A., Xu, X., Simpson, D., Schultz, M. G., Lefohn, A. S., Hamad, S., Moolla, R., Solberg, S., and Feng, Z.: Tropospheric Ozone Assessment Report: Present-day ozone distribution and

trends relevant to human health, Elem. Sci. Anth., 6, 12, https://doi.org/10.1525/elementa.273, 2018.

Fonseca, M. G., Anderson, L. O., Arai, E., Shimabukuro, Y. E., Xaud, H. A. M., Xaud, M. R., Madani, N., Wagner, F. H., and Aragão, L. E. O. C.: Climatic and anthropogenic drivers of northern Amazon fires during the 2015–2016 El Niño event, Ecol. Appl., 27, 2514–2527, https://doi.org/10.1002/eap.1628, 2017.

Gaubert, B., Emmons, L. K., Raeder, K., Tilmes, S., Miyazaki, K., Arellano Jr., A. F., Elguindi, N., Granier, C., Tang, W., Barré, J., Worden, H. M., Buchholz, R. R., Edwards, D. P., Franke, P., Anderson, J. L., Saunois, M., Schroeder, J., Woo, J.-H., Simpson, I. J., Blake, D. R., Meinardi, S., Wennberg, P. O., Crounse, J., Teng, A., Kim, M., Dickerson, R. R., He, H., Ren, X., Pusede, S. E., and Diskin, G. S.: Correcting model biases of CO in East Asia: impact on oxidant distributions during KORUS-AQ, Atmos. Chem. Phys., 20, 14617–14647, https://doi.org/10.5194/acp-20-14617-2020, 2020.

Gaudel, A., Cooper, O. R., Ancellet, G., Barret, B., Boynard, A., Burrows, J. P., Clerbaux, C., Coheur, P. F., Cuesta, J., Cuevas, E., Doniki, S., Dufour, G., Ebojie, F., Foret, G., Garcia, O., Granados-Muñoz, M. J., Hannigan, J. W., Hase, F., Hassler, B., Huang, G., Hurtmans, D., Jaffe, D., Jones, N., Kalabokas, P., Kerridge, B., Kulawik, S., Latter, B., Leblanc, T., Le Flochmoën, E., Lin, W., Liu, J., Liu, X., Mahieu, E., McClure-Begley, A., Neu, J. L., Osman, M., Palm, M., Petetin, H., Petropavlovskikh, I., Querel, R., Rahpoe, N., Rozanov, A., Schultz, M. G., Schwab, J., Siddans, R., Smale, D., Steinbacher, M., Tanimoto, H., Tarasick, D. W., Thouret, V., Thompson, A. M., Trickl, T., Weatherhead, E., Wespes, C., Worden, H. M., Vigouroux, C., Xu, X., Zeng, G., and Ziemke, J.: Tropospheric Ozone Assessment Report: Present-day distribution and trends of tropospheric ozone relevant to climate and global atmospheric chemistry model evaluation, Elem. Sci. Anth., 6, 39, https://doi.org/10.1525/elementa.291, 2018.

Gaudel, A., Cooper, O. R., Chang, K.-L., Bourgeois, I., Ziemke, J. R., Strode, S. A., Oman, L. D., Sellitto, P., Nédélec, P., Blot, R., Thouret, V., and Granier, C.: Aircraft observations since the 1990s reveal increases of tropospheric ozone at multiple locations across the Northern Hemisphere, Sci. Adv., 6, eaba8272, https://doi.org/10.1126/sciadv.aba8272, 2020.

Gelaro, R., McCarty, W., Su?rez, M. J., Todling, R., Molod, A., Takacs, L., Randles, C. A., Darmenov, A., Bosilovich, M. G., Reichle, R., Wargan, K., Coy, L., Cullather, R., Draper, C., Akella, S., Buchard, V., Conaty, A., da Silva, A. M., Gu, W., Kim, G.-K., Koster, R., Lucchesi, R., Merkova, D., Nielsen, J. E., Partyka, G., Pawson, S., Putman, W., Rienecker, M., Schubert, S. D., Sienkiewicz, M., and Zhao, B.: The Modern-Era Retrospective Analysis for Research and Applications, Version 2 (MERRA-2), J. Climate, 30, 5419–5454, https://doi.org/10.1175/JCLI-D-16-0758.1, 2017.

Global Modeling and Assimilation Office (GMAO): MERRA-2 tavgM_2d_slv_Nx: 2d,Monthly mean,Time-Averaged,Single-Level,Assimilation,Single-Level Diagnostics V5.12.4, Greenbelt, MD, USA, Goddard Earth Sciences Data and Information Services Center (GES DISC) [data set], https://doi.org/10.5067/AP1B0BA5PD2K, 2015.

GMAO: Modern-Era Retrospective analysis for Research and Applications, Version 2, GMAO [data set], http://geoschemdata.wustl.edu/ExtData/GEOS_4x5/MERRA2/, last access: 16 October 2022.

Griffiths, P. T., Keeble, J., Shin, Y. M., Abraham, N. L., Archibald, A. T., and Pyle, J. A.: On the Changing Role of the Stratosphere on the Tropospheric Ozone Budget: 1979–2010, Geophys. Res. Lett., 47, e2019GL086901, https://doi.org/10.1029/2019GL086901, 2020.

Griffiths, P. T., Murray, L. T., Zeng, G., Shin, Y. M., Abraham, N. L., Archibald, A. T., Deushi, M., Emmons, L. K., Galbally, I. E., Hassler, B., Horowitz, L. W., Keeble, J., Liu, J., Moeini, O., Naik, V., O'Connor, F. M., Oshima, N., Tarasick, D., Tilmes, S., Turnock, S. T., Wild, O., Young, P. J., and Zanis, P.: Tropospheric ozone in CMIP6 simulations, Atmos. Chem. Phys., 21, 4187–4218, https://doi.org/10.5194/acp-21-4187-2021, 2021.

Guenther, A. B., Jiang, X., Heald, C. L., Sakulyanontvittaya, T., Duhl, T., Emmons, L. K., and Wang, X.: The Model of Emissions of Gases and Aerosols from Nature version 2.1 (MEGAN2.1): an extended and updated framework for modeling biogenic emissions, Geosci. Model Dev., 5, 1471–1492, https://doi.org/10.5194/gmd-5-1471-2012, 2012.

Gulev, S. K., Thorne, P. W., Ahn, J., Dentener, F. J., Domingues, C. M., Gerland, S., Gong, D., Kaufman, D. S., Nnamchi, H. C., Quaas, J., Rivera, J. A., Sathyendranath, S., Smith, S. L., Trewin, B., Schuckmann, K. V., and Vose, R. S.: Changing state of the climate system, in: Climate Change 2021: The Physical Science Basis. Contribution of Working Group I to the Sixth Assessment Report of the Intergovernmental Panel on Climate Change, Cambridge University Press, Cambridge, United Kingdom and New York, NY, USA, 2021.

Hansen, J., Sato, M., and Ruedy, R.: Radiative forcing and climate response, J. Geophys. Res.-Atmos., 102, 6831–6864, https://doi.org/10.1029/96JD03436, 1997.

Hoesly, R. M., Smith, S. J., Feng, L., Klimont, Z., Janssens-Maenhout, G., Pitkanen, T., Seibert, J. J., Vu, L., Andres, R. J., Bolt, R. M., Bond, T. C., Dawidowski, L., Kholod, N., Kurokawa, J.-I., Li, M., Liu, L., Lu, Z., Moura, M. C. P., O'Rourke, P. R., and Zhang, Q.: Historical (1750–2014) anthropogenic emissions of reactive gases and aerosols from the Community Emissions Data System (CEDS), Geosci. Model Dev., 11, 369–408, https://doi.org/10.5194/gmd-11-369-2018, 2018.

Holmes, C. D., Bertram, T. H., Confer, K. L., Graham, K. A., Ronan, A. C., Wirks, C. K., and Shah, V.: The Role of Clouds in the Tropospheric NO_x Cycle: A New Modeling Approach for Cloud Chemistry and Its Global Implications, Geophys. Res. Lett., 46, 4980–4990, https://doi.org/10.1029/2019GL081990, 2019.

Hsu, J. and Prather, M. J.: Is the residual vertical velocity a good proxy for stratosphere-troposphere exchange of ozone?, Geophys. Res. Lett., 41, 9024–9032, https://doi.org/10.1002/2014GL061994, 2014.

Hu, L., Jacob, D. J., Liu, X., Zhang, Y., Zhang, L., Kim, P. S., Sulprizio, M. P., and Yantosca, R. M.: Global budget of tropospheric ozone: Evaluating recent model advances with satellite (OMI), aircraft (IAGOS), and ozonesonde observations, Atmos. Environ., 167, 323–334, https://doi.org/10.1016/j.atmosenv.2017.08.036, 2017.

Hudman, R. C., Russell, A. R., Valin, L. C., and Cohen, R. C.: Interannual variability in soil nitric oxide emissions over the United States as viewed from space, Atmos. Chem. Phys., 10, 9943–9952, https://doi.org/10.5194/acp-10-9943-2010, 2010.

Hudman, R. C., Moore, N. E., Mebust, A. K., Martin, R. V., Russell, A. R., Valin, L. C., and Cohen, R. C.: Steps towards a mechanistic model of global soil nitric oxide emissions: implementation and space based-constraints, Atmos. Chem. Phys., 12, 7779–7795, https://doi.org/10.5194/acp-12-7779-2012, 2012.

IAGOS: IAGOS-CORE, IAGOS-MOZAIC, IAGOS-CARIBIC [data set], https://iagos.aeris-data.fr/download/, last access: 16 October 2022.

Iglesias-Suarez, F., Kinnison, D. E., Rap, A., Maycock, A. C., Wild, O., and Young, P. J.: Key drivers of ozone change and its radiative forcing over the 21st century, Atmos. Chem. Phys., 18, 6121–6139, https://doi.org/10.5194/acp-18-6121-2018, 2018.

IPCC: Climate Change 2021: The Physical Science Basis. Contribution of Working Group I to the Sixth Assessment Report of the Intergovernmental Panel on Climate Change, edited by: Masson-Delmotte, V., Zhai, P., Pirani, A., Connors, S. L., Péan, C., Berger, S., Caud, N., Chen, Y., Goldfarb, L., Gomis, M. I., Huang, M., Leitzell, K., Lonnoy, E., Matthews, J. B. R., Maycock, T. K., Waterfield, T., Yelekçi, O., Yu, R., and Zhou, B., Cambridge University Press, Cambridge, United Kingdom and New York, NY, USA, in press, https://doi.org/10.1017/9781009157896, 2021.

IUPAC: Task group on atmospheric chemical kinetic data evaluation by International Union of Pure and Applied Chemistry (IUPAC), http://iupac.pole-ether.fr/ (last access: 30 May 2022), 2013.

Jacob, D. J.: Heterogeneous chemistry and tropospheric ozone, Atmos. Environ., 34, 2131–2159, https://doi.org/10.1016/S1352-2310(99)00462-8, 2000.

Keller, C. A., Long, M. S., Yantosca, R. M., Da Silva, A. M., Pawson, S., and Jacob, D. J.: HEMCO v1.0: a versatile, ESMF-compliant component for calculating emissions in atmospheric models, Geosci. Model Dev., 7, 1409–1417, https://doi.org/10.5194/gmd-7-1409-2014, 2014.

Koenker, R. and Hallock, K. F.: Quantile Regression, J. Econ. Perspect., 15, 143–156, https://doi.org/10.1257/jep.15.4.143, 2001.

Koenker, R. and Xiao, Z.: Inference on the Quantile Regression Process, Econometrica, 70, 1583–1612, https://doi.org/10.1111/1468-0262.00342, 2002.

Koenker, R. W. and Bassett Jr., G.: Regression Quantiles, Econometrica, 46, 33–50, https://doi.org/10.2307/1913643, 1978.

Krasting, J. P., John, J. G., Blanton, C., McHugh, C., Nikonov, S., Radhakrishnan, A., Rand, K., Zadeh, N. T., Balaji, V., Durachta, J., Dupuis, C., Menzel, R., Robinson, T., Underwood, S., Vahlenkamp, H., Dunne, K. A., Gauthier, P. P. G., Ginoux, P., Griffies, S. M., Hallberg, R., Harrison, M., Hurlin, W., Malyshev, S., Naik, V., Paulot, F., Paynter, D. J., Ploshay, J., Reichl, B. G., Schwarzkopf, D. M., Seman, C. J., Silvers, L., Wyman, B., Zeng, Y., Adcroft, A., Dunne, J. P., Dussin, R., Guo, H., He, J., Held, I. M., Horowitz, L. W., Lin, P., Milly, P. C. D., Shevliakova, E., Stock, C., Winton, M., Wittenberg, A. T., Xie, Y., and Zhao, M.: NOAA-GFDL GFDL-ESM4 model output prepared for CMIP6 CMIP historical, Earth System Grid Federation [data set], https://doi.org/10.22033/ESGF/CMIP6.8597, 2018.

Kumar, P., Kuttippurath, J., von der Gathen, P., Petropavlovskikh, I., Johnson, B., McClure-Begley, A., Cristofanelli, P., Bonasoni, P., Barlasina, M. E., and Sánchez, R.: The Increasing Surface Ozone and Tropospheric Ozone in Antarctica and Their Possible Drivers, Environ. Sci. Technol., 55, 8542–8553, https://doi.org/10.1021/acs.est.0c08491, 2021.

Kurokawa, J., Ohara, T., Morikawa, T., Hanayama, S., Janssens-Maenhout, G., Fukui, T., Kawashima, K., and Akimoto, H.: Emissions of air pollutants and greenhouse gases over Asian regions during 2000–2008: Regional Emission inventory in ASia (REAS) version 2, Atmos. Chem. Phys., 13, 11019–11058, https://doi.org/10.5194/acp-13-11019-2013, 2013.

Lacis, A. A., Wuebbles, D. J., and Logan, J. A.: Radiative forcing of climate by changes in the vertical distribution of ozone, J. Geophys. Res.-Atmos., 95, 9971–9981, https://doi.org/10.1029/JD095iD07p09971, 1990.

Lawrence, M. G., Rasch, P. J., von Kuhlmann, R., Williams, J., Fischer, H., de Reus, M., Lelieveld, J., Crutzen, P. J., Schultz, M., Stier, P., Huntrieser, H., Heland, J., Stohl, A., Forster, C., Elbern, H., Jakobs, H., and Dickerson, R. R.: Global chemical weather forecasts for field campaign planning: predictions and observations of large-scale features during MINOS, CONTRACE, and INDOEX, Atmos. Chem. Phys., 3, 267–289, https://doi.org/10.5194/acp-3-267-2003, 2003.

Lee, D. S., Fahey, D. W., Skowron, A., Allen, M. R., Burkhardt, U., Chen, Q., Doherty, S. J., Freeman, S., Forster, P. M., Fuglestvedt, J., Gettelman, A., De León, R. R., Lim, L. L., Lund, M. T., Millar, R. J., Owen, B., Penner, J. E., Pitari, G., Prather, M. J., Sausen, R., and Wilcox, L. J.: The contribution of global aviation to anthropogenic climate forcing for 2000 to 2018, Atmos. Environ., 244, 117834, https://doi.org/10.1016/j.atmosenv.2020.117834, 2021.

Li, M., Zhang, Q., Kurokawa, J.-I., Woo, J.-H., He, K., Lu, Z., Ohara, T., Song, Y., Streets, D. G., Carmichael, G. R., Cheng, Y., Hong, C., Huo, H., Jiang, X., Kang, S., Liu, F., Su, H., and Zheng, B.: MIX: a mosaic Asian anthropogenic emission inventory under the international collaboration framework of the MICS-Asia and HTAP, Atmos. Chem. Phys., 17, 935–963, https://doi.org/10.5194/acp-17-935-2017, 2017.

Lin, J.-T. and McElroy, M. B.: Impacts of boundary layer mixing on pollutant vertical profiles in the lower troposphere: Implications to satellite remote sensing, Atmos. Environ., 44, 1726–1739, https://doi.org/10.1016/j.atmosenv.2010.02.009, 2010.

Lin, M., Horowitz, L. W., Oltmans, S. J., Fiore, A. M., and Fan, S.: Tropospheric ozone trends at Mauna Loa Observatory tied to decadal climate variability, Nat. Geosci., 7, 136–143, https://doi.org/10.1038/ngeo2066, 2014.

Lin, M., Horowitz, L. W., Payton, R., Fiore, A. M., and Tonnesen, G.: US surface ozone trends and extremes from 1980 to 2014: quantifying the roles of rising Asian emissions, domestic controls, wildfires, and climate, Atmos. Chem. Phys., 17, 2943–2970, https://doi.org/10.5194/acp-17-2943-2017, 2017.

Lin, S.-J. and Rood, R. B.: Multidimensional Flux-Form Semi-Lagrangian Transport Schemes, Mon. Weather Rev., 124, 2046–2070, https://doi.org/10.1175/1520-0493(1996)124<2046:MFFSLT>2.0.CO;2, 1996.

Liu, H., Jacob, D. J., Bey, I., and Yantosca, R. M.: Constraints from 210Pb and 7Be on wet deposition and transport in a global three-dimensional chemical tracer model driven by assimilated meteorological fields, J. Geophys. Res.-Atmos., 106, 12109–12128, https://doi.org/10.1029/2000JD900839, 2001.

Lu, X., Zhang, L., Liu, X., Gao, M., Zhao, Y., and Shao, J.: Lower tropospheric ozone over India and its linkage to the South Asian monsoon, Atmos. Chem. Phys., 18, 3101–3118, https://doi.org/10.5194/acp-18-3101-2018, 2018.

Lu, X., Zhang, L., and Shen, L.: Meteorology and Climate Influences on Tropospheric Ozone: a Review of Natural Sources, Chemistry, and Transport Patterns, Curr. Poll. Rep., 5, 238–260, https://doi.org/10.1007/s40726-019-00118-3, 2019a.

Lu, X., Zhang, L., Zhao, Y., Jacob, D. J., Hu, Y., Hu, L., Gao, M., Liu, X., Petropavlovskikh, I., McClure-Begley, A., and Querel, R.: Surface and tropospheric ozone trends in the Southern Hemisphere since 1990: possible linkages to poleward expansion of the Hadley circulation, Sci. Bull., 64, 400–409, https://doi.org/10.1016/j.scib.2018.12.021, 2019b.

Lu, X., Ye, X., Zhou, M., Zhao, Y., Weng, H., Kong, H., Li, K., Gao, M., Zheng, B., Lin, J., Zhou, F., Zhang, Q., Wu, D., Zhang, L., and Zhang, Y.: The underappreciated role of agricultural soil nitrogen oxide emissions in ozone pollution regulation in North China, Nat. Commun., 12, 5021, https://doi.org/10.1038/s41467-021-25147-9, 2021.

Mao, J., Fan, S., Jacob, D. J., and Travis, K. R.: Radical loss in the atmosphere from Cu-Fe redox coupling in aerosols, Atmos. Chem. Phys., 13, 509–519, https://doi.org/10.5194/acp-13-509-2013, 2013.

Marais, E. A. and Wiedinmyer, C.: Air Quality Impact of Diffuse and Inefficient Combustion Emissions in Africa (DICE-Africa), Environ. Sci. Technol., 50, 10739–10745, https://doi.org/10.1021/acs.est.6b02602, 2016.

McDuffie, E. E., Smith, S. J., O'Rourke, P., Tibrewal, K., Venkataraman, C., Marais, E. A., Zheng, B., Crippa, M., Brauer, M., and Martin, R. V.: A global anthropogenic emission inventory of atmospheric pollutants from sector- and fuel-specific sources (1970–2017): an application of the Community Emissions Data System (CEDS), Earth Syst. Sci. Data, 12, 3413–3442, https://doi.org/10.5194/essd-12-3413-2020, 2020.

Meinshausen, M., Vogel, E., Nauels, A., Lorbacher, K., Meinshausen, N., Etheridge, D. M., Fraser, P. J., Montzka, S. A., Rayner, P. J., Trudinger, C. M., Krummel, P. B., Beyerle, U., Canadell, J. G., Daniel, J. S., Enting, I. G., Law, R. M., Lunder, C. R., O'Doherty, S., Prinn, R. G., Reimann, S., Rubino, M., Velders, G. J. M., Vollmer, M. K., Wang, R. H. J., and Weiss, R.: Historical greenhouse gas concentrations for climate modelling (CMIP6), Geosci. Model Dev., 10, 2057–2116, https://doi.org/10.5194/gmd-10-2057-2017, 2017.

Monks, P. S., Archibald, A. T., Colette, A., Cooper, O., Coyle, M., Derwent, R., Fowler, D., Granier, C., Law, K. S., Mills, G. E., Stevenson, D. S., Tarasova, O., Thouret, V., von Schneidemesser, E., Sommariva, R., Wild, O., and Williams, M. L.: Tropospheric ozone and its precursors from the urban to the global scale from air quality to short-lived climate forcer, Atmos. Chem. Phys., 15, 8889–8973, https://doi.org/10.5194/acp-15-8889-2015, 2015.

Murray, L. T., Jacob, D. J., Logan, J. A., Hudman, R. C., and Koshak, W. J.: Optimized regional and interannual variability of lightning in a global chemical transport model constrained by LIS/OTD satellite data, J. Geophys. Res.-Atmos., 117, D20307, https://doi.org/10.1029/2012JD017934, 2012.

Murray, L. T.: Lightning NO_x and Impacts on Air Quality, Curr. Poll. Rep., 2, 115–133, https://doi.org/10.1007/s40726-016-0031-7, 2016.

Myhre, G. and Stordal, F.: Role of spatial and temporal variations in the computation of radiative forcing and GWP, J. Geophys. Res.-Atmos., 102, 11181–11200, https://doi.org/10.1029/97JD00148, 1997.

Myhre, G., Shine, K. P., Rädel, G., Gauss, M., Isaksen, I. S. A., Tang, Q., Prather, M. J., Williams, J. E., van Velthoven, P., Dessens, O., Koffi, B., Szopa, S., Hoor, P., Grewe, V., Borken-Kleefeld, J., Berntsen, T. K., and Fuglestvedt, J. S.: Radiative forcing due to changes in ozone and methane caused by the transport sector, Atmos. Environ., 45, 387–394, https://doi.org/10.1016/j.atmosenv.2010.10.001, 2011.

Nédélec, P., Blot, R., Boulanger, D., Athier, G., Cousin, J.-M., Gautron, B., Petzold, A., Volz-Thomas, A., and Thouret, V.: Instrumentation on commercial aircraft for monitoring the atmospheric composition on a global scale: the IAGOS system, technical overview of ozone and carbon monoxide measurements, Tellus B, 67, 27791, https://doi.org/10.3402/tellusb.v67.27791, 2015.

Neubauer, D., Ferrachat, S., Siegenthaler-Le Drian, C., Stoll, J., Folini, D. S., Tegen, I., Wieners, K.-H., Mauritsen, T., Stemmler, I., Barthel, S., Bey, I., Daskalakis, N., Heinold, B., Kokkola, H., Partridge, D., Rast, S., Schmidt, H., Schutgens, N., Stanelle, T., Stier, P., Watson-Parris, D., and Lohmann, U.: HAMMOZ-Consortium MPI-ESM1.2-HAM model output prepared for CMIP6 AerChemMIP, Earth System Grid Federation [data set], https://doi.org/10.22033/ESGF/CMIP6.1621, 2019.

Nowak, J. B., Parrish, D. D., Neuman, J. A., Holloway, J. S., Cooper, O. R., Ryerson, T. B., Nicks Jr., D. K., Flocke, F., Roberts, J. M., Atlas, E., de Gouw, J. A., Donnelly, S., Dunlea, E., Hübler, G., Huey, L. G., Schauffler, S., Tanner, D. J., Warneke, C., and Fehsenfeld, F. C.: Gas-phase chemical characteristics of Asian emission plumes observed during ITCT 2K2 over the eastern North Pacific Ocean, J. Geophys. Res.-Atmos., 109, D23S19, https://doi.org/10.1029/2003JD004488, 2004.

O'Rourke, P. R., Smith, S. J., Mott, A., Ahsan, H., McDuffie, E. E., Crippa, M., Klimont, Z., McDonald, B., Wang, S. X., Nicholson, M. B., Feng, L., and Hoesly, R. M.: CEDS v-2021-04-21 Emission Data 1975-2019 (Version Apr-21-2021), https://data.pnnl.gov/dataset/CEDS-4-21-21 (last access: 30 May 2022), 2021.

Oltmans, S. J., Lefohn, A. S., Shadwick, D., Harris, J. M., Scheel, H. E., Galbally, I., Tarasick, D. W., Johnson, B. J., Brunke, E. G., Claude, H., Zeng, G., Nichol, S., Schmidlin, F., Davies, J., Cuevas, E., Redondas, A., Naoe, H., Nakano, T., and Kawasato, T.: Recent tropospheric ozone changes – A pattern dominated by slow or no growth, Atmos. Environ., 67, 331–351, https://doi.org/10.1016/j.atmosenv.2012.10.057, 2013.

O'Rourke, P. R., Smith, S. J., Mott, A., Ahsan, H., McDuffie, E. E., Crippa, M., Klimont, Z., McDonald, B., Wang, S. X., Nicholson, M. B., Feng, L., and Hoesly, R. M.: CEDS v-2021-04-21 Emission Data 1975-2019 (Version Apr-21-2021) [data set], https://data.pnnl.gov/dataset/CEDS-4-21-21 (last access: 30 May 2022), 2021.

Ott, L. E., Pickering, K. E., Stenchikov, G. L., Allen, D. J., DeCaria, A. J., Ridley, B., Lin, R.-F., Lang, S., and Tao, W.-K.: Production of lightning NO_x and its vertical distribution calculated from three-dimensional cloud-scale chemical transport model simulations, J. Geophys. Res.-Atmos., 115, D04301, https://doi.org/10.1029/2009JD011880, 2010.

Park, R. J., Jacob, D. J., Field, B. D., Yantosca, R. M., and Chin, M.: Natural and transboundary pollution influences on sulfate-nitrate-ammonium aerosols in the United States: Implications for policy, J. Geophys. Res.-Atmos., 109, D15204, https://doi.org/10.1029/2003JD004473, 2004.

Park, R. J., Oak, Y. J., Emmons, L. K., Kim, C.-H., Pfister, G. G., Carmichael, G. R., Saide, P. E., Cho, S.-Y., Kim, S., Woo, J.-H., Crawford, J. H., Gaubert, B., Lee, H.-J., Park, S.-Y., Jo, Y.-J., Gao, M., Tang, B., Stanier, C. O., Shin, S. S., Park, H. Y., Bae, C., and Kim, E.: Multi-model intercomparisons of air quality simulations for the KORUS-AQ campaign, Elem. Sci. Anth., 9, 00139, https://doi.org/10.1525/elementa.2021.00139, 2021.

Parrella, J. P., Jacob, D. J., Liang, Q., Zhang, Y., Mickley, L. J., Miller, B., Evans, M. J., Yang, X., Pyle, J. A., Theys, N., and Van Roozendael, M.: Tropospheric bromine chemistry: implications for present and pre-industrial ozone and mercury, Atmos. Chem. Phys., 12, 6723–6740, https://doi.org/10.5194/acp-12-6723-2012, 2012.

Parrish, D. D., Lamarque, J.-F., Naik, V., Horowitz, L., Shindell, D. T., Staehelin, J., Derwent, R., Cooper, O. R., Tanimoto, H., Volz-Thomas, A., Gilge, S., Scheel, H.-E., Steinbacher, M., and Fröhlich, M.: Long-term changes in lower tropospheric baseline ozone concentrations: Comparing chemistry-climate models and observations at northern midlatitudes, J. Geophys. Res.-Atmos., 119, 5719–5736, https://doi.org/10.1002/2013JD021435, 2014.

Petetin, H., Thouret, V., Athier, G., Blot, R., Boulanger, D., Cousin, J. M., Gaudel, A., Nédélec, P., and Cooper, O.: Diurnal cycle of ozone throughout the troposphere over Frankfurt as measured by MOZAIC-IAGOS commercial aircraft, Elem. Sci. Anth., 4, 000129, https://doi.org/10.12952/journal.elementa.000129, 2016.

Petetin, H., Jeoffrion, M., Sauvage, B., Athier, G., Blot, R., Boulanger, D., Clark, H., Cousin, J. M., Gheusi, F., Nedelec, P., Steinbacher, M., and Thouret, V.: Representativeness of the IAGOS airborne measurements in the lower troposphere, Elem. Sci. Anth., 6, 23, https://doi.org/10.1525/elementa.280, 2018.

Petzold, A., Thouret, V., Gerbig, C., Zahn, A., Brenninkmeijer, C. A. M., Gallagher, M., Hermann, M., Pontaud, M., Ziereis, H., Boulanger, D., Marshall, J., Nédélec, P., Smit, H. G. J., Friess, U., Flaud, J.-M., Wahner, A., Cammas, J.-P., and Volz-Thomas, A.: Global-scale atmosphere monitoring by in-service aircraft – current achievements and future prospects of the European Research Infrastructure IAGOS, Tellus B, 67, 28452, https://doi.org/10.3402/tellusb.v67.28452, 2015.

Pound, R. J., Sherwen, T., Helmig, D., Carpenter, L. J., and Evans, M. J.: Influences of oceanic ozone deposition on tropospheric photochemistry, Atmos. Chem. Phys., 20, 4227–4239, https://doi.org/10.5194/acp-20-4227-2020, 2020.

Price, C. and Rind, D.: A simple lightning parameterization for calculating global lightning distributions, J. Geophys. Res.-Atmos., 97, 9919–9933, https://doi.org/10.1029/92JD00719, 1992.

Qu, Z., Henze, D. K., Cooper, O. R., and Neu, J. L.: Impacts of global NO_x inversions on NO_2 and ozone simulations, Atmos. Chem. Phys., 20, 13109–13130, https://doi.org/10.5194/acp-20-13109-2020, 2020.

Rap, A., Richards, N. A. D., Forster, P. M., Monks, S. A., Arnold, S. R., and Chipperfield, M. P.: Satellite constraint on the tropospheric ozone radiative effect, Geophys. Res. Lett., 42, 5074–5081, https://doi.org/10.1002/2015GL064037, 2015.

Sander, S. P., Golden, D., Kurylo, M., Moortgat, G., Wine, P., Ravishankara, A., Kolb, C., Molina, M., Finlayson-Pitts, B., and Huie, R.: Chemical kinetics and photochemical data for use in atmospheric studies, JPL Publ., 684 pp., 2011.

Sauvage, B., Martin, R. V., van Donkelaar, A., Liu, X., Chance, K., Jaeglé, L., Palmer, P. I., Wu, S., and Fu, T.-M.: Remote sensed and in situ constraints on processes affecting tropical tropospheric ozone, Atmos. Chem. Phys., 7, 815–838, https://doi.org/10.5194/acp-7-815-2007, 2007.

Schultz, M. G., Schröder, S., Lyapina, O., Cooper, O. R., Galbally, I., Petropavlovskikh, I., von Schneidemesser, E., Tanimoto, H., Elshorbany, Y., Naja, M., Seguel, R. J., Dauert, U., Eckhardt, P., Feigenspan, S., Fiebig, M., Hjellbrekke, A.-G., Hong, Y.-D., Kjeld, P. C., Koide, H., Lear, G., Tarasick, D., Ueno, M., Wallasch, M., Baumgardner, D., Chuang, M.-T., Gillett, R., Lee, M., Molloy, S., Moolla, R., Wang, T., Sharps, K., Adame, J. A., Ancellet, G., Apadula, F., Artaxo, P., Barlasina, M. E., Bogucka, M., Bonasoni, P., Chang, L., Colomb, A., Cuevas-Agulló, E., Cupeiro, M., Degorska, A., Ding, A., Fröhlich, M., Frolova, M., Gadhavi, H., Gheusi, F., Gilge, S., Gonzalez, M. Y., Gros, V., Hamad, S. H., Helmig, D., Henriques, D., Hermansen, O., Holla, R., Hueber, J., Im, U., Jaffe, D. A., Komala, N., Kubistin, D., Lam, K.-S., Laurila, T., Lee, H., Levy, I., Mazzoleni, C., Mazzoleni, L. R., McClure-Begley, A., Mohamad, M., Murovec, M., Navarro-Comas, M., Nicodim, F., Parrish, D., Read, K. A., Reid, N., Ries, L., Saxena, P., Schwab, J. J., Scorgie, Y., Senik, I., Simmonds, P., Sinha, V., Skorokhod, A. I., Spain, G., Spangl, W., Spoor, R., Springston, S. R., Steer, K., Steinbacher, M., Suharguniyawan, E., Torre, P., Trickl, T., Weili, L., Weller, R., Xiaobin, X., Xue, L., and Zhiqiang, M.: Tropospheric Ozone Assessment Report: Database and metrics data of global surface ozone observations, Elem. Sci. Anth., 5, 58, https://doi.org/10.1525/elementa.244, 2017.

Scott, C. E., Monks, S. A., Spracklen, D. V., Arnold, S. R., Forster, P. M., Rap, A., Äijälä, M., Artaxo, P., Carslaw, K. S., Chipperfield, M. P., Ehn, M., Gilardoni, S., Heikkinen, L., Kulmala, M., Petäjä, T., Reddington, C. L. S., Rizzo, L. V., Swietlicki, E., Vignati, E., and Wilson, C.: Impact on short-lived climate forcers increases projected warming due to deforestation, Nat. Commun., 9, 157, https://doi.org/10.1038/s41467-017-02412-4, 2018.

Sherwen, T., Schmidt, J. A., Evans, M. J., Carpenter, L. J., Großmann, K., Eastham, S. D., Jacob, D. J., Dix, B., Koenig, T. K., Sinreich, R., Ortega, I., Volkamer, R., Saiz-Lopez, A., Prados-Roman, C., Mahajan, A. S., and Ordóñez, C.: Global impacts of tropospheric halogens (Cl, Br, I) on oxidants and composition in GEOS-Chem, Atmos. Chem. Phys., 16, 12239–12271, https://doi.org/10.5194/acp-16-12239-2016, 2016.

Silvern, R. F., Jacob, D. J., Travis, K. R., Sherwen, T., Evans, M. J., Cohen, R. C., Laughner, J. L., Hall, S. R., Ullmann, K., Crounse, J. D., Wennberg, P. O., Peischl, J., and Pollack, I. B.: Observed NO/NO2 Ratios in the Upper Troposphere Imply Errors in NO-NO_2-O_3 Cycling Kinetics or an Unaccounted NO_x Reservoir, Geophys. Res. Lett., 45, 4466–4474, https://doi.org/10.1029/2018GL077728, 2018.

Simon, H., Reff, A., Wells, B., Xing, J., and Frank, N.: Ozone Trends Across the United States over a Period of Decreasing NO_x and VOC Emissions, Environ. Sci. Technol., 49, 186–195, https://doi.org/10.1021/es504514z, 2015.

Skeie, R. B., Myhre, G., Hodnebrog, Ø., Cameron-Smith, P. J., Deushi, M., Hegglin, M. I., Horowitz, L. W., Kramer, R. J., Michou, M., Mills, M. J., Olivié, D. J. L., Connor, F. M. O., Paynter, D., Samset, B. H., Sellar, A., Shindell, D., Takemura, T., Tilmes, S., and Wu, T.: Historical total ozone radiative forcing

derived from CMIP6 simulations, npj Clim. Atmos. Sci., 3, 32, https://doi.org/10.1038/s41612-020-00131-0, 2020.

Solomon, S., Ivy Diane, J., Kinnison, D., Mills Michael, J., Neely Ryan, R., and Schmidt, A.: Emergence of healing in the Antarctic ozone layer, Science, 353, 269–274, https://doi.org/10.1126/science.aae0061, 2016.

Stamnes, K., Tsay, S. C., Wiscombe, W., and Jayaweera, K.: Numerically stable algorithm for discrete-ordinate-method radiative transfer in multiple scattering and emitting layered media, Appl. Opt., 27, 2502–2509, https://doi.org/10.1364/AO.27.002502, 1988.

Staufer, J., Staehelin, J., Stübi, R., Peter, T., Tummon, F., and Thouret, V.: Trajectory matching of ozonesondes and MOZAIC measurements in the UTLS – Part 1: Method description and application at Payerne, Switzerland, Atmos. Meas. Tech., 6, 3393–3406, https://doi.org/10.5194/amt-6-3393-2013, 2013.

Staufer, J., Staehelin, J., Stübi, R., Peter, T., Tummon, F., and Thouret, V.: Trajectory matching of ozonesondes and MOZAIC measurements in the UTLS – Part 2: Application to the global ozonesonde network, Atmos. Meas. Tech., 7, 241–266, https://doi.org/10.5194/amt-7-241-2014, 2014.

Steinbrecht, W., Kubistin, D., Plass-Dülmer, C., Davies, J., Tarasick, D. W., Gathen, P. v. d., Deckelmann, H., Jepsen, N., Kivi, R., Lyall, N., Palm, M., Notholt, J., Kois, B., Oelsner, P., Allaart, M., Piters, A., Gill, M., Van Malderen, R., Delcloo, A. W., Sussmann, R., Mahieu, E., Servais, C., Romanens, G., Stübi, R., Ancellet, G., Godin-Beekmann, S., Yamanouchi, S., Strong, K., Johnson, B., Cullis, P., Petropavlovskikh, I., Hannigan, J. W., Hernandez, J.-L., Diaz Rodriguez, A., Nakano, T., Chouza, F., Leblanc, T., Torres, C., Garcia, O., Röhling, A. N., Schneider, M., Blumenstock, T., Tully, M., Paton-Walsh, C., Jones, N., Querel, R., Strahan, S., Stauffer, R. M., Thompson, A. M., Inness, A., Engelen, R., Chang, K.-L., and Cooper, O. R.: COVID-19 Crisis Reduces Free Tropospheric Ozone Across the Northern Hemisphere, Geophys. Res. Lett., 48, e2020GL091987, https://doi.org/10.1029/2020GL091987, 2021.

Sterling, C. W., Johnson, B. J., Oltmans, S. J., Smit, H. G. J., Jordan, A. F., Cullis, P. D., Hall, E. G., Thompson, A. M., and Witte, J. C.: Homogenizing and estimating the uncertainty in NOAA's long-term vertical ozone profile records measured with the electrochemical concentration cell ozonesonde, Atmos. Meas. Tech., 11, 3661–3687, https://doi.org/10.5194/amt-11-3661-2018, 2018.

Stevenson, D. S., Young, P. J., Naik, V., Lamarque, J.-F., Shindell, D. T., Voulgarakis, A., Skeie, R. B., Dalsoren, S. B., Myhre, G., Berntsen, T. K., Folberth, G. A., Rumbold, S. T., Collins, W. J., MacKenzie, I. A., Doherty, R. M., Zeng, G., van Noije, T. P. C., Strunk, A., Bergmann, D., Cameron-Smith, P., Plummer, D. A., Strode, S. A., Horowitz, L., Lee, Y. H., Szopa, S., Sudo, K., Nagashima, T., Josse, B., Cionni, I., Righi, M., Eyring, V., Conley, A., Bowman, K. W., Wild, O., and Archibald, A.: Tropospheric ozone changes, radiative forcing and attribution to emissions in the Atmospheric Chemistry and Climate Model Intercomparison Project (ACCMIP), Atmos. Chem. Phys., 13, 3063–3085, https://doi.org/10.5194/acp-13-3063-2013, 2013.

Szopa, S., Naik, V., Adhikary, B., Artaxo, P., Berntsen, T., Collins, W. D., Fuzzi, S., Gallardo, L., Scharr, A. K., Klimont, Z., Liao, H., Unger, N., and Zanis, P.: Short-Lived Climate Forcers, in: Climate Change 2021: The Physical Science Basis, Contribution of Working Group I to the Sixth Assessment Report of the Intergovernmental Panel on Climate Change, Cambridge University Press, Cambridge, United Kingdom and New York, NY, USA, https://doi.org/10.1017/9781009157896.008, 2021.

Tarasick, D., Galbally, I. E., Cooper, O. R., Schultz, M. G., Ancellet, G., Leblanc, T., Wallington, T. J., Ziemke, J., Liu, X., Steinbacher, M., Staehelin, J., Vigouroux, C., Hannigan, J. W., García, O., Foret, G., Zanis, P., Weatherhead, E., Petropavlovskikh, I., Worden, H., Osman, M., Liu, J., Chang, K.-L., Gaudel, A., Lin, M., Granados-Muñoz, M., Thompson, A. M., Oltmans, S. J., Cuesta, J., Dufour, G., Thouret, V., Hassler, B., Trickl, T., and Neu, J. L.: Tropospheric Ozone Assessment Report: Tropospheric ozone from 1877 to 2016, observed levels, trends and uncertainties, Elem. Sci. Anth., 7, 39, https://doi.org/10.1525/elementa.376, 2019.

Tarasick, D. W., Davies, J., Smit, H. G. J., and Oltmans, S. J.: A re-evaluated Canadian ozonesonde record: measurements of the vertical distribution of ozone over Canada from 1966 to 2013, Atmos. Meas. Tech., 9, 195–214, https://doi.org/10.5194/amt-9-195-2016, 2016.

Thouret, V., Marenco, A., Logan, J. A., Nédélec, P., and Grouhel, C.: Comparisons of ozone measurements from the MOZAIC airborne program and the ozone sounding network at eight locations, J. Geophys. Res.-Atmos., 103, 25695–25720, https://doi.org/10.1029/98JD02243, 1998.

Travis, K. R., Jacob, D. J., Fisher, J. A., Kim, P. S., Marais, E. A., Zhu, L., Yu, K., Miller, C. C., Yantosca, R. M., Sulprizio, M. P., Thompson, A. M., Wennberg, P. O., Crounse, J. D., St. Clair, J. M., Cohen, R. C., Laughner, J. L., Dibb, J. E., Hall, S. R., Ullmann, K., Wolfe, G. M., Pollack, I. B., Peischl, J., Neuman, J. A., and Zhou, X.: Why do models overestimate surface ozone in the Southeast United States?, Atmos. Chem. Phys., 16, 13561–13577, https://doi.org/10.5194/acp-16-13561-2016, 2016.

Unger, N., Zheng, Y., Yue, X., and Harper, K. L.: Mitigation of ozone damage to the world's land ecosystems by source sector, Nat. Clim. Change, 10, 134–137, https://doi.org/10.1038/s41558-019-0678-3, 2020.

US EPA: Air Pollutant Emissions Trends Data: Average Annual Emissions, https://www.epa.gov/sites/production/files/2015-07/national_tier1_caps.xlsx (last access: 30 May 2022), 2016.

US EPA: National Annual Emissions Trend: 1970–2018, https://www.epa.gov/air-emissions-inventories/air-pollutant-emissions-trends-data (last access: 30 May 2022), 2019.

van der Werf, G. R., Dempewolf, J., Trigg, S. N., Randerson, J. T., Kasibhatla, P. S., Giglio, L., Murdiyarso, D., Peters, W., Morton, D. C., Collatz, G. J., Dolman, A. J., and DeFries, R. S.: Climate regulation of fire emissions and deforestation in equatorial Asia, P. Natl. Acad. Sci. USA, 105, 20350–20355, https://doi.org/10.1073/pnas.0803375105, 2008.

van der Werf, G. R., Randerson, J. T., Giglio, L., van Leeuwen, T. T., Chen, Y., Rogers, B. M., Mu, M., van Marle, M. J. E., Morton, D. C., Collatz, G. J., Yokelson, R. J., and Kasibhatla, P. S.: Global fire emissions estimates during 1997–2016, Earth Syst. Sci. Data, 9, 697–720, https://doi.org/10.5194/essd-9-697-2017, 2017.

van Marle, M. J. E., Kloster, S., Magi, B. I., Marlon, J. R., Daniau, A.-L., Field, R. D., Arneth, A., Forrest, M., Hantson, S., Kehrwald, N. M., Knorr, W., Lasslop, G., Li, F., Mangeon, S., Yue, C., Kaiser, J. W., and van der Werf, G. R.: His-

toric global biomass burning emissions for CMIP6 (BB4CMIP) based on merging satellite observations with proxies and fire models (1750–2015), Geosci. Model Dev., 10, 3329–3357, https://doi.org/10.5194/gmd-10-3329-2017, 2017.

Venkataraman, C., Brauer, M., Tibrewal, K., Sadavarte, P., Ma, Q., Cohen, A., Chaliyakunnel, S., Frostad, J., Klimont, Z., Martin, R. V., Millet, D. B., Philip, S., Walker, K., and Wang, S.: Source influence on emission pathways and ambient $PM_{2.5}$ pollution over India (2015–2050), Atmos. Chem. Phys., 18, 8017–8039, https://doi.org/10.5194/acp-18-8017-2018, 2018.

Wang, M. and Fu, Q.: Stratosphere-Troposphere Exchange of Air Masses and Ozone Concentrations Based on Reanalyses and Observations, J. Geophys. Res.-Atmos., 126, e2021JD035159, https://doi.org/10.1029/2021JD035159, 2021.

Wang, X., Jacob, D. J., Downs, W., Zhai, S., Zhu, L., Shah, V., Holmes, C. D., Sherwen, T., Alexander, B., Evans, M. J., Eastham, S. D., Neuman, J. A., Veres, P. R., Koenig, T. K., Volkamer, R., Huey, L. G., Bannan, T. J., Percival, C. J., Lee, B. H., and Thornton, J. A.: Global tropospheric halogen (Cl, Br, I) chemistry and its impact on oxidants, Atmos. Chem. Phys., 21, 13973–13996, https://doi.org/10.5194/acp-21-13973-2021, 2021.

Wang, Y., Jacob, D. J., and Logan, J. A.: Global simulation of tropospheric O3-NO_x-hydrocarbon chemistry: 1. Model formulation, J. Geophys. Res.-Atmos., 103, 10713–10725, https://doi.org/10.1029/98JD00158, 1998.

Wasserstein, R. L., Schirm, A. L., and Lazar, N. A.: Moving to a World Beyond "$p < 0.05$", The American Statistician, 73, 1–19, https://doi.org/10.1080/00031305.2019.1583913, 2019.

Weber, M., Arosio, C., Coldewey-Egbers, M., Fioletov, V. E., Frith, S. M., Wild, J. D., Tourpali, K., Burrows, J. P., and Loyola, D.: Global total ozone recovery trends attributed to ozone-depleting substance (ODS) changes derived from five merged ozone datasets, Atmos. Chem. Phys., 22, 6843–6859, https://doi.org/10.5194/acp-22-6843-2022, 2022.

Wesely, M. L.: Parameterization of surface resistances to gaseous dry deposition in regional-scale numerical models, Atmos. Environ., 23, 1293–1304, https://doi.org/10.1016/0004-6981(89)90153-4, 1989.

Wild, O. and Prather, M. J.: Global tropospheric ozone modeling: Quantifying errors due to grid resolution, J. Geophys. Res.-Atmos., 111, D11305, https://doi.org/10.1029/2005JD006605, 2006.

Witte, J. C., Thompson, A. M., Smit, H. G. J., Fujiwara, M., Posny, F., Coetzee, G. J. R., Northam, E. T., Johnson, B. J., Sterling, C. W., Mohamad, M., Ogino, S.-Y., Jordan, A., and da Silva, F. R.: First reprocessing of Southern Hemisphere ADditional OZonesondes (SHADOZ) profile records (1998–2015): 1. Methodology and evaluation, J. Geophys. Res.-Atmos., 122, 6611–6636, https://doi.org/10.1002/2016JD026403, 2017.

Witte, J. C., Thompson, A. M., Smit, H. G. J., Vömel, H., Posny, F., and Stübi, R.: First Reprocessing of Southern Hemisphere ADditional OZonesondes Profile Records: 3. Uncertainty in Ozone Profile and Total Column, J. Geophys. Res.-Atmos., 123, 3243–3268, https://doi.org/10.1002/2017JD027791, 2018.

World Ozone and Ultraviolet Radiation Data Centre: Data, WOUDC [data set], https://woudc.org/data.php, last access: 16 October 2022.

Wu, T., Zhang, F., Zhang, J., Jie, W., Zhang, Y., Wu, F., Li, L., Yan, J., Liu, X., Lu, X., Tan, H., Zhang, L., Wang, J., and Hu, A.: Beijing Climate Center Earth System Model version 1 (BCC-ESM1): model description and evaluation of aerosol simulations, Geosci. Model Dev., 13, 977–1005, https://doi.org/10.5194/gmd-13-977-2020, 2020.

Xu, W., Xu, X., Lin, M., Lin, W., Tarasick, D., Tang, J., Ma, J., and Zheng, X.: Long-term trends of surface ozone and its influencing factors at the Mt Waliguan GAW station, China – Part 2: The roles of anthropogenic emissions and climate variability, Atmos. Chem. Phys., 18, 773–798, https://doi.org/10.5194/acp-18-773-2018, 2018.

Yan, Y., Pozzer, A., Ojha, N., Lin, J., and Lelieveld, J.: Analysis of European ozone trends in the period 1995–2014, Atmos. Chem. Phys., 18, 5589–5605, https://doi.org/10.5194/acp-18-5589-2018, 2018.

Yang, Y., Liao, H., and Li, J.: Impacts of the East Asian summer monsoon on interannual variations of summertime surface-layer ozone concentrations over China, Atmos. Chem. Phys., 14, 6867–6879, https://doi.org/10.5194/acp-14-6867-2014, 2014.

Yin, H., Lu, X., Sun, Y., Li, K., Gao, M., Zheng, B., and Liu, C.: Unprecedented decline in summertime surface ozone over eastern China in 2020 comparably attributable to anthropogenic emission reductions and meteorology, Environ. Res. Lett., 16, 124069, https://doi.org/10.1088/1748-9326/ac3e22, 2021.

Young, P. J., Naik, V., Fiore, A. M., Gaudel, A., Guo, J., Lin, M. Y., Neu, J. L., Parrish, D. D., Rieder, H. E., Schnell, J. L., Tilmes, S., Wild, O., Zhang, L., Ziemke, J., Brandt, J., Delcloo, A., Doherty, R. M., Geels, C., Hegglin, M. I., Hu, L., Im, U., Kumar, R., Luhar, A., Murray, L., Plummer, D., Rodriguez, J., Saiz-Lopez, A., Schultz, M. G., Woodhouse, M. T., and Zeng, G.: Tropospheric Ozone Assessment Report: Assessment of global-scale model performance for global and regional ozone distributions, variability, and trends, Elem. Sci. Anth., 6, 10, https://doi.org/10.1525/elementa.265, 2018.

Yu, K., Jacob, D. J., Fisher, J. A., Kim, P. S., Marais, E. A., Miller, C. C., Travis, K. R., Zhu, L., Yantosca, R. M., Sulprizio, M. P., Cohen, R. C., Dibb, J. E., Fried, A., Mikoviny, T., Ryerson, T. B., Wennberg, P. O., and Wisthaler, A.: Sensitivity to grid resolution in the ability of a chemical transport model to simulate observed oxidant chemistry under high-isoprene conditions, Atmos. Chem. Phys., 16, 4369–4378, https://doi.org/10.5194/acp-16-4369-2016, 2016.

Zeng, G. and Pyle, J. A.: Influence of El Niño Southern Oscillation on stratosphere/troposphere exchange and the global tropospheric ozone budget, Geophys. Res. Lett., 32, L01814, https://doi.org/10.1029/2004GL021353, 2005.

Zeng, G., Morgenstern, O., Shiona, H., Thomas, A. J., Querel, R. R., and Nichol, S. E.: Attribution of recent ozone changes in the Southern Hemisphere mid-latitudes using statistical analysis and chemistry–climate model simulations, Atmos. Chem. Phys., 17, 10495–10513, https://doi.org/10.5194/acp-17-10495-2017, 2017.

Zhang, L., Gong, S., Padro, J., and Barrie, L.: A size-segregated particle dry deposition scheme for an atmospheric aerosol module, Atmos. Environ., 35, 549–560, https://doi.org/10.1016/S1352-2310(00)00326-5, 2001.

Zhang, L., Jacob, D. J., Yue, X., Downey, N. V., Wood, D. A., and Blewitt, D.: Sources contributing to background surface ozone in the US Intermountain West, Atmos. Chem. Phys., 14, 5295–5309, https://doi.org/10.5194/acp-14-5295-2014, 2014.

Zhang, Y., Cooper, O. R., Gaudel, A., Thompson, A. M., Nédélec, P., Ogino, S.-Y., and West, J. J.: Tropospheric ozone change from 1980 to 2010 dominated by equatorward redistribution of emissions, Nat. Geosci., 9, 875–879, https://doi.org/10.1038/ngeo2827, 2016.

Zhang, Y., West, J. J., Emmons, L. K., Flemming, J., Jonson, J. E., Lund, M. T., Sekiya, T., Sudo, K., Gaudel, A., Chang, K.-L., Nédélec, P., and Thouret, V.: Contributions of World Regions to the Global Tropospheric Ozone Burden Change From 1980 to 2010, Geophys. Res. Lett., 48, e2020GL089184, https://doi.org/10.1029/2020GL089184, 2021.

Zheng, B., Tong, D., Li, M., Liu, F., Hong, C., Geng, G., Li, H., Li, X., Peng, L., Qi, J., Yan, L., Zhang, Y., Zhao, H., Zheng, Y., He, K., and Zhang, Q.: Trends in China's anthropogenic emissions since 2010 as the consequence of clean air actions, Atmos. Chem. Phys., 18, 14095–14111, https://doi.org/10.5194/acp-18-14095-2018, 2018.

Ziemke, J. R., Oman, L. D., Strode, S. A., Douglass, A. R., Olsen, M. A., McPeters, R. D., Bhartia, P. K., Froidevaux, L., Labow, G. J., Witte, J. C., Thompson, A. M., Haffner, D. P., Kramarova, N. A., Frith, S. M., Huang, L.-K., Jaross, G. R., Seftor, C. J., Deland, M. T., and Taylor, S. L.: Trends in global tropospheric ozone inferred from a composite record of TOMS/OMI/MLS/OMPS satellite measurements and the MERRA-2 GMI simulation, Atmos. Chem. Phys., 19, 3257–3269, https://doi.org/10.5194/acp-19-3257-2019, 2019.